Received 2 July 2024; accepted 17 July 2024. Date of publication 19 July 2024; date of current version 29 July 2024.

Digital Object Identifier 10.1109/OJCOMS.2024.3431273

Design and Performance Analysis of Multirate-NOMA

HAMAD YAHYA [1,2] (Member, IEEE), EMAD ALSUSA [3] (Senior Member, IEEE), AND ARAFAT AL-DWEIK [4,5] (Senior Member, IEEE)

[1]Department of Electrical Engineering, Khalifa University of Science and Technology, Abu Dhabi, UAE

[2]Department of Electrical and Electronic Engineering, Imperial College London, SW7 2AZ London, U.K.

[3]Department of Electrical and Electronic Engineering, The University of Manchester, M13 9PL Manchester, U.K.

[4]Department of Computer and Information Engineering, Khalifa University of Science and Technology, Abu Dhabi, UAE

[5]6G Research Centre, Khalifa University of Science and Technology, Abu Dhabi, UAE

CORRESPONDING AUTHOR: H. YAHYA (e-mail: hamad.myahya@ku.ac.ae)

ABSTRACT Non-orthogonal multiple access (NOMA) is a promising candidate to improve the spectral efficiency by multiplexing users in the power-domain. Most of the work in the literature considers the analysis of the single-rate (SR)-NOMA, which can only vary the power per user, limiting its flexibility and bit error rate (BER) performance. Therefore, this work considers the design and performance analysis of multirate (MR)-NOMA, which controls the symbol energy per user by varying the symbol rate and power simultaneously. Both joint-multiuser maximum likelihood sequence detector (JMLSD) based on the maximum liklihood criterion and a novel low-complexity optimal successive interference cancellation (SIC) receiver are designed. Furthermore, closed-form BER expressions are derived considering arbitrary symbol rates and modulation orders. The derived expressions are then used to optimize the power allocation at the base station (BS) to minimize the BER while strictly satisfying certain BER requirements. The presented results show that MR-NOMA offers more trade-off freedom between spectral efficiency and robustness to errors. As such, MR-NOMA can have up to two orders of magnitude improvement in BER performance in some scenarios. The derived expressions are validated via simulations.

INDEX TERMS Joint-multiuser maximum likelihood sequence detector (JMLSD), multirate communications, non-orthogonal multiple access (NOMA), power allocation, successive interference cancellation (SIC).

I. INTRODUCTION

With rapid growth on the demand for higher capacity wireless communication systems and more efficient spectrum utilization, NOMA has attracted much attention as it can improve spectral efficiency, support massive connectivity, and enable users with diverse quality of service (QoS) requirements to communicate simultaneously [1]. NOMA can be classified into power-domain and code-domain [2]. Power-domain NOMA multiplexes users in the power-domain by allocating users different power coefficients [3], [4]. Nonetheless, code-domain NOMA allocates users different codes that are not necessarily orthogonal [4]. Therefore, multiuser interference is inherent in NOMA because of the superposition coding (SC) of different users' signals. Such interference can be mitigated at the users' ends using SIC [2]. Beyond cellular communication, orthogonal and non-orthogonal schemes have been integrated into satellite-terrestrial, satellite-aerial-terrestrial, and intelligent reflecting surface (IRS)-aided communication systems, demonstrating significant advancements [5], [6], [7], [8].

A. RELATED WORK

Since legacy one-size-fits-all systems do not meet the diverse requirements of future wireless networks, multinumerology NOMA [9], [10], [11], [12], [13], partial NOMA [14], [15], [16], [17], [18], [19], [20], [21], [22], and multirate NOMA [23], [24] are introduced to meet the envisioned requirements of enhanced mobile broadband (eMBB), ultra-reliable low latency communications (uRLLC) and massive machine-type communications (mMTC). The characteristics and traits of these systems are highlighted and discussed in detail subsequently.

Multinumerology NOMA: Multinumerologies are introduced for multicarrier systems such as orthogonal frequency-division multiplexing (OFDM) to adopt various subcarrier spacing based on the requirements of the application, and hence, the symbols can have different durations. While different numerologies can be multiplexed in time/frequency domains [25], multinumerology NOMA multiplexes the numerologies in power-domain leading to severe inter-numerology interference forming a performance bottleneck. Multinumerology NOMA has been studied by a number of researchers focusing on the inter-numerology interference problem, e.g., [9], [10], [11], [12], [13]. McWade et al. [9] explored the uplink (UL) two-user scenarios using SIC to combat inter-numerology interference. An expression is derived for the inter-numerology interference at each user to analyze the spectral efficiency. Exhaustive search is used to find the optimal power allocation that maximizes the spectral efficiency for two different SIC orders. The authors extended the work in [10] by generalizing the model to an arbitrary number of users and optimizing the subcarrier and power allocations to maximize spectral efficiency. On the other hand, Choi et al. [11] explored a downlink (DL) two-user system with time-domain SC, and derived the inter-numerology interference distribution to approximate the symbol error rate (SER). The problem of high peak-to-average-power ratio of multinumerology NOMA is tackaled in [12] by introducing selected mapping. The authors of [13] derived the average inter-numerology interference in the presence of phase noise in terms of the channel's power delay profile at each subcarrier.

Partial NOMA: Similar to multinumerology NOMA, partial NOMA is introduced for multicarrier systems but the subcarrier spacing is kept the same for all users. Partial NOMA controls the multiuser interference by controlling the extent of the frequency overlap between users. Partial NOMA systems are studied for DL in [14], [15], [16], [18] considering Gaussian signalling to evaluate the impact of frequency overlapping ratio on the multiuser interference and the sum rate. Kim et al. [14] provided the signal to interference and noise ratio (SINR) for the two-user partial NOMA system and derived sum rate expressions. It is shown that partial NOMA achieves a better sum rate when compared to orthogonal multiple access (OMA) or fully overlapped NOMA systems. Similarly, they considered user fairness as a performance metric in [15]. Ali et al. [16], [17] studied two-user partial NOMA in a multi-cell environment. Using stochastic geometry, they analyzed the rate region for a novel SIC receiver and formulated an optimization problem to maximize the cell sum rate while satisfying the individual users' rates. Zhuo et al. [18] investigated IRS aided partial NOMA for a two-user scenario, and derived closed-form bounds of the achievable rates. Furthermore, the role of partial NOMA in improving physical layer security is studied in [19], [20], [21] for different settings. For instance, Ali et al. [20] considered large-cell and proposed receive-filtering followed by flexible SIC to improve the secrecy probability. The authors of [19] proposed four cooperative relaying schemes and derived the achievable secrecy rates. In addition, they proposed enhanced decoding protocols to improve the secrecy outage probability in [21]. Furthermore, the authors of [22] analyzed the performance of partial NOMA for integrated-sensing and communication.

Multirate-NOMA: Unlike multinumerology and partial NOMA systems, multirate (MR)-NOMA is proposed for the single-carrier systems. $^{[R_{2,3}]}$ While the single-rate (SR)-NOMA fixes the symbol rates for all users, MR-NOMA assigns the users different symbol rates based on their requirements. Hence, the users experience different overlaps in the frequency/time-domain. Specifically, longer symbols duration are assigned for massive delay-tolerant devices to allow reliable detection, whereas delay-sensitive applications such as vehicle-to-vehicle communication are assigned shorter symbol durations due to their stringent latency requirements. Numerical results of the bit error rate (BER) for UL MR-NOMA has been presented in [23], [24] without analytical derivations. For instance, multilevel irregular repeat-accumulate channel coding is considered in [23], while [24] considers uncoded scenario with arbitrary symbol rates.

B. MOTIVATIONS AND CONTRIBUTIONS

Despite the capacity advantage of SR-NOMA, its main drawback is the error rate performance degradation due to the multiuser interference. Because all users have equal symbol rates, the power allocation for the SR-NOMA users is performed while considering their distances from the base station (BS) [26]. Hence, the design flexibility and error rate performance of SR-NOMA are limited by two degrees of freedom which are the modulation orders and power allocation. Consequently, this article analyzes the error rate performance of the MR-NOMA presented in [24], which incorporates the symbol rate and exploites its relation with the symbol power and energy to introduce a new degree of freedom, where the power allocation for the MR-NOMA users is performed based on their distances and their symbol rates. Hence, the multiuser interference can be controlled to achieve certain BER requirements.

The main contributions of this article can be summarized as follows:

1) Propose a DL MR-NOMA where the users are assigned arbitrary modulation orders and symbol rates.
2) Design the optimal detector for the system using the maximum likelihood criterion and derive an upper bound on its BER based on the pair-wise error probability (PEP) and union bound.
3) Design a low-complexity MR-SIC detector and derive the exact BER for the low-rate user while an accurate approximation and upper/lower bounds are derived for the high-rate user.

4) Formulate an optimization problem to minimize one of the users' BER while satisfying the QoS requirements of the other. The obtained results show that the optimum power allocation can be significantly relaxed when the symbol duration of the low-rate user is much longer than the high-rate user.
5) Provide numerical results and quantify the BER performance gain of MR-NOMA over SR-NOMA. The obtained results show that the BER of both users can be reduced by optimizing the energy of the low-rate user.

C. ARTICLE ORGANIZATION

The remaining content of the article is organized as follows. In Section II, the system and channel models are introduced. Sections III and IV present the BER performance analysis of the optimal and low-complexity detectors, respectively. In addition, Section IV presents the power allocation to minimize the system's BER while satisfying some QoS requirements. Section V presents the analytical and Monte-Carlo simulation results. Finally, Section VI concludes the article.

D. NOTATIONS

The notations used throughout the article are as follows. Boldface uppercase and lowercase symbols such as $\mathbf{X}$ and $\mathbf{x}$ will denote matrix and column/row vectors, respectively. The transpose and the Hermitian transpose are denoted by $(\cdot)^\top$ and $(\cdot)^H$. The set of complex numbers and integers are denoted by $\mathbb{C}$ and $\mathbb{Z}$. $\Pr(\cdot)$ is the probability of an event, $f(\cdot)$ is the probability density function (PDF) of a random variable, $\mathbb{E}[\cdot]$ is the statistical expectation, $|\cdot|$ is the absolute value, $\|\cdot\|_2$ is the Euclidean norm, $\mathrm{Re}[\cdot]$ and $\mathrm{Im}[\cdot]$ denote the real and imaginary components, $\lfloor\cdot\rfloor$ is the flooring function, $\binom{n}{k}_s$ denotes the generalized binomial coefficients of order s, $\binom{n}{k}_2$ denotes the binomial coefficients, $\binom{n}{k_1,k_2,\ldots,k_N}$ denotes the multinomial coefficients. The identity $N\times N$ matrix is denoted as I_N, while $\mathbf{1}_N$ denotes the column vector of ones with length N. The normal and complex normal random variables with a zero mean and σ^2 variance are denoted as $\mathcal{N}(0,\sigma^2)$ and $\mathcal{CN}(0,\sigma^2)$. The Gaussian Q-function is denoted by $Q(x)\triangleq\frac{1}{\sqrt{2\pi}}\int_x^\infty \exp\left(-\frac{u^2}{2}\right)\mathrm{d}u$.

II. SYSTEM AND CHANNEL MODELS

A. SIGNAL MODEL

In this work, we consider a downlink MR-NOMA system with N users being assigned different symbol rates, where the normalized symbol duration is denoted by T_n s and $n\in\{1,2,\ldots,N\}$. Without loss of generality, T_n is ordered as $T_1<T_2<\cdots<T_N$, where T_1 is associated with the highest symbol rate user U_1, which is nearest to the BS. T_N is associated with the lowest symbol rate user U_N, which is farthest from the BS. Note that there is a constraint on T_n to unify the sampling rate at the receivers such that $\frac{T_N}{T_n}\triangleq\tau_n\in\mathbb{Z}$ [24]. Without loss of generality, we consider the normalized symbol period $T_1=1$. Therefore, the transmitted signal can be written as

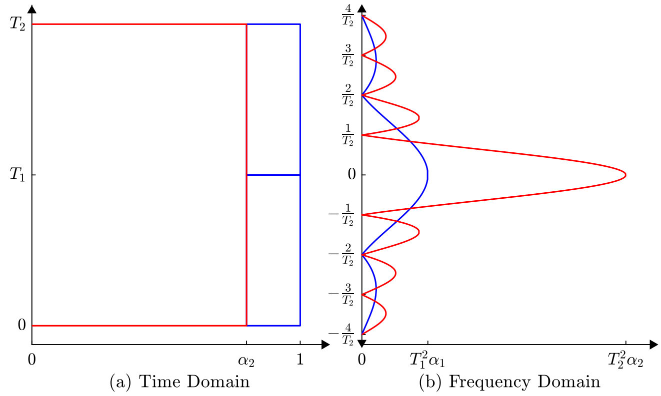

FIGURE 1. Time domain signal power and frequency domain signal energy for $N=2$, where square pulses are assumed in time-domain and $T_2=2T_1$.

$$x[\ell]=\sum\nolimits_{n=1}^{N}\sqrt{\alpha_n}x_n[\ell],\ \ell\in\{1,2,\ldots,T_N\} \tag{1}$$

where $x_n[\ell]$ is the nth user data symbol at the ℓth sample time. The data symbols belong to a binary phase-shift keying (BPSK) or quadrature amplitude modulation (QAM) constellation χ_n, where the nth user modulation order is M_n, $\mathcal{M}_n=\log_2 M_n$ represents the bits/symbol, the modulation orders vector is defined as $\mathfrak{m}=[M_1,M_2,\ldots,M_N]$. The bit rate is defined as $R_n=\mathcal{M}_n/T_n$, and α_n is the nth user power coefficient, $\sum_{n=1}^{N}\alpha_n=1$ and the power coefficients are assigned such that $\alpha_1<\alpha_2<\cdots<\alpha_N$ to allow reliable detection at the users' ends [27], [28]. Besides, the symbol rate assignment and power allocation are motivated by the fact that the far user is both interference-limited and suffers from more severe signal attenuation due to large-scale fading. Therefore, achieving a reliable BER performance for the far user requires allocating a higher power coefficient and lower symbol rate. It is worth noting that we assume $\mathbb{E}[|x[\ell]|^2]=\mathbb{E}[|x_n[\ell]|^2]=1$ to ensure a normalized symbol energy at each instance. Fig. 1 shows the signal power in the time domain and the signal energy in frequency domain for a two-user scenario with $T_2=2T_1$, where square pulses are assumed in the time-domain. As can be seen from (1), the transmitted baseband signal corresponds to a single-carrier with rectangular pulse shape, which is a widely used configuration in the absence of time alignment [2]. In the presence of time or frequency alignment, other pulse shapes should be considered [29], [30], [31], [32].

During a window of T_N signaling periods, the transmitted signal forms a sequence, $\mathbf{x}\in\mathbb{C}^{T_N\times 1}$, which can be written as

$$\mathbf{x}=\sum_{n=1}^{N}\sqrt{\alpha_n}\mathbf{x}_n \tag{2}$$

where $\mathbf{x}=[x[1],x[2],\ldots,x[T_N]]^\top$ and the structure of $\mathbf{x}_n$ depends on T_n and τ_n. That is, during a T_N window, U_n will have τ_n different data symbols spread uniformly over

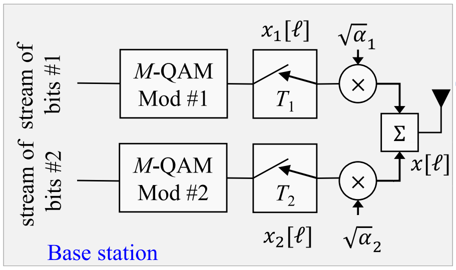

FIGURE 2. The MR-NOMA BS block diagram for $N = 2$.

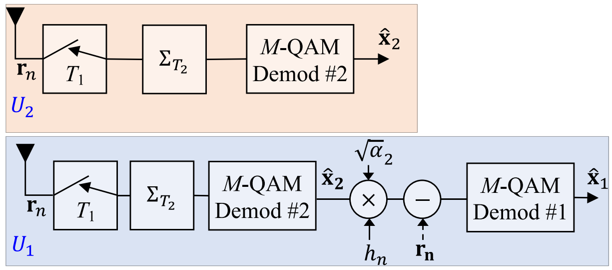

FIGURE 3. The proposed detector block diagram for $N = 2$.

the sequence $\mathbf{x}$. For example, for $N = 2, T_1 = 1$, and $T_2 = 2$, $\mathbf{x}_1 = [x_1[1], x_1[2]]^\top$ where $x_1[1] \not\Longleftrightarrow x_1[2]$, and $\mathbf{x}_2 = [x_2[1], x_2[2]]^\top$ where $x_2[1] \Longleftrightarrow x_2[2]$. Thus,

$$x[1] = \sqrt{\alpha_1}x_1[1] + \sqrt{\alpha_2}x_2[1] \tag{3}$$
$$x[2] = \sqrt{\alpha_1}x_1[2] + \sqrt{\alpha_2}x_2[2]. \tag{4}$$

The MR-NOMA transmitter is shown in Fig. 2 for $N = 2$. In this figure, two different QAM modulators are used where the first has modulation order M_1 while the second has modulation order M_2. The sampling rates of the modulators are not necessarily equal because the symbol rates can be different. The bit rates for each modulator can also be different.

By considering that all users' receivers have a unified sampling frequency of $F_s = 1/T_1$, the received sequence at the nth user receiver can be expressed as

$$\mathbf{r}_n = h_n\mathbf{x} + \mathbf{w}_n \tag{5}$$

where h_n is the channel gain, the additive white Gaussian noise (AWGN) vector $\mathbf{w}_n = [w_n[1], w_n[2], \ldots, w_n[T_N]]^\top \sim \mathcal{CN}(0, N_0\mathbf{I}_{T_N})$, and N_0 is the power spectral density.

B. RECEIVER MODEL

By noting that the received signal can be modeled as a sequence, then its PDF for a given h_n and trial sequence $\tilde{\mathbf{x}}$ would follow a multivariate complex Gaussian PDF,

$$f(\mathbf{r}_n; h_n, \mathbf{x} = \tilde{\mathbf{x}}) = \frac{1}{(\pi N_0)^{T_N}} \exp\left(\frac{-1}{N_0}\|\mathbf{r}_n - h_n\tilde{\mathbf{x}}\|_2^2\right). \tag{6}$$

Consequently, the optimal detector, JMLSD, after some straightforward manipulations, can be expressed as

$$\begin{aligned}\{\hat{\mathbf{x}}_1, \ldots, \hat{\mathbf{x}}_N\} &= \arg\max_{\tilde{\mathbf{x}}} f(\mathbf{r}_n; h_n, \mathbf{x} = \tilde{\mathbf{x}}) \\ &= \arg\max_{\tilde{\mathbf{x}}} \exp\left(-\|\mathbf{r}_n - h_n\tilde{\mathbf{x}}\|_2^2\right) \\ &= \arg\min_{\tilde{\mathbf{x}}} \|\mathbf{r}_n - h_n\tilde{\mathbf{x}}\|_2^2. \end{aligned} \tag{7}$$

When all users have identical symbol rates, the JMLSD simplifies to a symbol-by-symbol joint-multiuser maximum likelihood detector (JMLD).

C. PROPOSED MR-SIC LOW COMPLEXITY DETECTOR

By noting that $\{\alpha_N > \alpha_n, T_N > T_n\}$ $\forall n < N$, then the detection order is $x_N, x_{N-1}, \ldots, x_1$. Fig. 3 shows the proposed detector for $N = 2$. As shown in this figure, U_2 detects its own symbol directly and stops. For U_1, it has to detect $\mathbf{x}_2$ first, then apply SIC and detect $\mathbf{x}_1$. Therefore, U_1 should perform three demodulation operations. In terms of hardware implementation, the number of required modulators depends on the values of $[M_1, M_2]$ and the desired delay. For example, if $M_1 = M_2$ and the detection after SIC is performed sequentially, then only one detector is required. If $M_1 \neq M_2$, then two demodulators are required. In the worst-case scenario where $M_1 \neq M_2$ and parallel demodulation is performed after SIC three demodulators are required. Based on the structure of the T_N samples, the MR-SIC detector at U_n is a generalization of the SR-NOMA and can be expressed as follows:

Step 1: $\mathbf{x}_N$ detection. It can be detected by summing the samples received during T_N, and using a single-user maximum likelihood detector (MLD) such that the detected elements of $\mathbf{x}_N$ can be written as

$$\hat{x}_N[\ell] = \arg\min_{\tilde{x}_N}\left|\mathbf{1}_N^\top\mathbf{r}_n - h_n\sqrt{\alpha_N}T_N\tilde{x}_N\right|^2 \tag{8}$$

where $\hat{x}_N[1] = \hat{x}_N[2] = \cdots = \hat{x}_N[T_N]$ and $\mathbf{1}_N^\top\mathbf{r}_n = \sum_{i=1}^{T_N} r_n[i]$, $\mathbf{1}_N \in 1^{T_N\times 1}$.

Step 2: To detect $\mathbf{x}_n$ for $n < N$, SIC can be used recursively to eliminate interference from the higher energy symbols such that

$$\tilde{\mathbf{r}}_n = \mathbf{r}_n - h_n\sum_{i=n+1}^{N}\sqrt{\alpha_i}\hat{\mathbf{x}}_i. \tag{9}$$

Step 3: Vector partitioning should take place to fragment $\tilde{\mathbf{r}}_n$ into τ_n equal-sized vectors, i.e., $\tilde{\mathbf{r}}_n = [\tilde{\mathbf{r}}_n^1; \tilde{\mathbf{r}}_n^2; \ldots; \tilde{\mathbf{r}}_n^{\tau_n}]$ where $\tilde{\mathbf{r}}_n^j = [\tilde{r}_n[(j-1)T_n + 1], \ldots, \tilde{r}_n[jT_n]]^\top$.

Step 4: The elements of $\mathbf{x}_n$ can be detected after SIC using a single-user MLD,

$$\hat{x}_n[\ell] = \arg\min_{\tilde{x}_n}\left|\mathbf{1}_n^\top\tilde{\mathbf{r}}_n^k - h_n\sqrt{\alpha_n}T_n\tilde{x}_n\right|^2 \tag{10}$$

where $k = \lceil\frac{\ell}{T_n}\rceil$ and $\mathbf{1}_n \in 1^{T_n\times 1}$.

The detection process for U_n is summarized in Algorithm 1. According to the algorithm, it can be noted

Algorithm 1: MR-SIC Receiver Design for the U_n

Input: $n, h_n, \mathbf{r}_n, T_i, \alpha_i, M_i, \forall i \in \{n, n+1, \ldots, N\}$
Output: $\widehat{\mathbf{x}}_n$
1 Apply MLD to compute $\widehat{\mathbf{x}}_N$ using (8)
2 **if** $n < N$ **then**
3   **for** $i = N-1 : -1 : n$ **do**
4   Apply SIC to compute $\tilde{\mathbf{r}}_i$ using (9)
5   Partition $\tilde{\mathbf{r}}_i$ to generate $\tilde{\mathbf{r}}_i^j$, $\forall j \in \{1, 2, \ldots, \tau_i\}$
6   Apply MLD to compute $\widehat{\mathbf{x}}_i$ using (10)

that all users should share some of their system parameters to enable the MR-SIC to operate properly. This information includes α_i, T_i, and M_i for all users, which can be provided by the BS to all higher energy users, i.e., $i \geq n$. Therefore, in terms of scalability, if a new user joins or leaves the group, the users have to update their receivers with the new parameters, which is generally similar to SR-NOMA. Furthermore, the proposed low-complexity MR-SIC detector simplifies to the conventional SR-SIC detector when $T_n = 1$, $\forall n$. Specifically, the received signal at the nth user as shown in (5) becomes a scalar and can be explicitly written as in [2, eq. (1)]. Consequently, the sample time in (8) can be omitted. Thus, the single-user MLD in **Step 1** can be explicitly expressed as [2, eq. (2)]. Additionally, the SIC can proceed with the single-user MLD without vector partitioning. Therefore, (9) in **Step 2** and (10) in **Step 4** can be explicitly written as in [2, eq. (3)] by omitting **Step 3**.

It is worth noting that the computational complexity (CC) of the proposed MR-SIC is comparable to the conventional SR-SIC, which is significantly less than the JMLSD as will be shown in (11)–(12) and (13)–(14). In addition to its reduced complexity, it is shown in Section V that the JMLSD and the proposed MR-SIC offer equivalent BER performance, while the proof of equivalence is shown in Appendix A. The detailed CC analysis is given in the following subsection.

D. COMPLEXITY ANALYSIS

Generally, the MR-SIC and conventional SR-SIC have some common features such as the sequential detection and the necessity to detect other users' symbols. However, MR-SIC has some additional operations and requirements:

- Buffering and fragmentation: The users' signals are oversampled and hence, the samples should be buffered. Then, the buffered samples should be fragmented with different lengths as described in Algorithm 1. Such processes are not required for conventional SR-SIC.
- SIC requirements: In conventional SR-SIC, the nth user uses MLD $N - n$ times to detect other users symbols before detecting its own symbols. For MR-SIC, the number of times MLD is performed is greater, and can be expressed as $(N-n)\sum_{i=n}^{N} \tau_i$. The additional MLD operations may increase the delay if performed sequentially, and thus parallel MLD implementation can be useful to reduce the delay.
- Delay: For the highest symbol rate user U_1, although the receiver has to buffer τ_1 symbols before starting the detection process, since τ_1 is generally small, the delay is tolerable.
- Synchronization requirement: Because all users have to sample their signals at the symbol rate of U_1, then the timing synchronization should correspond to the smallest period T_1, which implies that the synchronization error should be quite small relative to T_1, which can incur some additional synchronization complexity for low-rate users.

The CC of the proposed MR-SIC is evaluated in terms of the number of real floating point addition (R_A) and multiplication (R_M) operations and compared to JMLSD. For JMLSD, the complexity can be derived based on (7), which can be simplified to (18) as will be shown in the next section. The complexity of (18) is due to the large sample space of the trail values $\tilde{\mathbf{x}}$, which is equal to $\prod_{i=1}^{N} M_i^{\tau_i}$. For a simple scenario of three users with $M_i = 4\ \forall i$ and $T_2 = 2$ and $T_3 = 4$, the sample space size is $M^7 = 16384$. For each trail sequence $\tilde{\mathbf{x}}$, the number of operations can be computed based on (18) which is a simplified version of (7). Although the norm $\|\tilde{\mathbf{x}}\|_2^2$ can be ignored because it can be computed once offline. However, its dependence on the power factor α_1 implies that the norm may be computed more frequently. Therefore, it is included in the CC to capture the worst-case scenario. Therefore,

$$CC_{\text{JMLSD}}^{RM} = (12 + 10T_N)\prod_{i=1}^{N} M_i^{\tau_i} \tag{11}$$

$$CC_{\text{JMLSD}}^{RA} = (11 + 7T_N)\prod_{i=1}^{N} M_i^{\tau_i}. \tag{12}$$

For MR-SIC detector, the CC can be computed based on the receiver design described in Section II-D. Unlike JMLSD, a single user MLD is used and thus the sample space increases linearly versus $\{M_i, \tau_i\}\ \forall i \geq n$. Consequently,

$$CC_{\text{MR-SIC}}^{RM} = (N-n)(4T_N + 2) + \sum_{i=n}^{N}(3 + 8M_i)\tau_i \tag{13}$$

$$CC_{\text{MR-SIC}}^{RA} = (N-n)(5T_N + 1) + \sum_{i=n}^{N}(2T_i + 6M_i + 3)\tau_i. \tag{14}$$

As can be noted from (13) and (14), the complexity depends on the user index where U_N will have the lowest complexity while U_1 will have the highest complexity. Even for the worst-case of $n = 1$, the complexity of the MR-SIC detector is significantly less than JMLSD. In addition, T_i and τ_i have a linear impact on the CC. Hence, MR-SIC has a comparable CC to SR-SIC.

III. BIT ERROR RATE ANALYSIS: JMLSD

This section derives the instantaneous BER of JMLSD in (7) for the two-user system while considering generalized symbol rates and modulation orders.

A. JMLSD DECISION METRIC ANALYSIS

For coherent detection, the decision variable $\acute{\varphi}_n$ is given by

$$\acute{\varphi}_n = \|\mathbf{r}_n - h_n\widetilde{\mathbf{x}}\|_2^2 = \left\|\mathbf{r}_n - |h_n|e^{j\theta_n}\widetilde{\mathbf{x}}\right\|_2^2 = \|\check{\mathbf{r}}_n - |h_n|\widetilde{\mathbf{x}}\|_2^2 \tag{15}$$

where $\check{\mathbf{r}}_n = |h_n|\mathbf{x} + \exp(-j\theta_n)\mathbf{w}_n$, $\exp(-j\theta_n)\mathbf{w}_n$ and $\mathbf{w}_n$ have similar statistical properties due to the circular symmetry of the AWGN. Using the identity

$$\begin{aligned}\|\mathbf{u} - \mathbf{v}\|_2^2 &= (\mathbf{u} + \mathbf{v})^H(\mathbf{u} - \mathbf{v}) \\ &= \|\mathbf{u}\|_2^2 + \|\mathbf{v}\|_2^2 - 2\mathrm{Re}\left[\mathbf{u}^H\mathbf{v}\right]\end{aligned} \tag{16}$$

$\acute{\varphi}_n$ simplifies to

$$\begin{aligned}\acute{\varphi}_n &= \|\check{\mathbf{r}}_n\|_2^2 + |h_n|^2\|\widetilde{\mathbf{x}}\|_2^2 - 2|h_n|\mathrm{Re}\left[\check{\mathbf{r}}_n^H\widetilde{\mathbf{x}}\right] \\ &= \|\check{\mathbf{r}}_n\|_2^2 + |h_n|^2\left(\|\widetilde{\mathbf{x}}\|_2^2 - \frac{2}{|h_n|}\mathrm{Re}\left[\check{\mathbf{r}}_n^H\widetilde{\mathbf{x}}\right]\right).\end{aligned} \tag{17}$$

Because $\|\check{\mathbf{r}}_n\|_2^2$ and $|h_n|^2$ are fixed for all terms, then they can be dropped, and the simplified decision variable can be expressed as

$$\begin{aligned}\varphi_n &= \|\widetilde{\mathbf{x}}\|_2^2 - \frac{2}{|h_n|}\mathrm{Re}\left[\check{\mathbf{r}}_n^H\widetilde{\mathbf{x}}\right] \\ &= \|\widetilde{\mathbf{x}}\|_2^2 - 2\mathrm{Re}\left[\left(\mathbf{x} + \frac{e^{-j\theta_n}}{|h_n|}\mathbf{w}_n\right)^H\widetilde{\mathbf{x}}\right].\end{aligned} \tag{18}$$

By defining $\mathbf{z} = \frac{\exp(-j\theta_n)\mathbf{w}_n}{|h_n|}$,

$$\begin{aligned}\varphi_n &= \|\widetilde{\mathbf{x}}\|_2^2 - 2\mathrm{Re}\left[(\mathbf{x} + \mathbf{z})^H\widetilde{\mathbf{x}}\right] \\ &= \|\widetilde{\mathbf{x}}\|_2^2 - 2\mathrm{Re}\left[\mathbf{x}^H\widetilde{\mathbf{x}}\right] - 2\mathrm{Re}\left[\mathbf{z}^H\widetilde{\mathbf{x}}\right].\end{aligned} \tag{19}$$

For a given $|h_n|$, $\mathbf{z} \sim \mathcal{CN}(0, \frac{N_0}{|h_n|^2}\mathbf{I}_{T_N})$. Consequently, $2\mathrm{Re}[\mathbf{z}^H\widetilde{\mathbf{x}}] \sim \mathcal{N}(0, \frac{N_0\|\widetilde{\mathbf{x}}\|_2^2}{|h_n|^2})$ and $\|\widetilde{\mathbf{x}}\|_2^2 - 2\mathrm{Re}[\mathbf{x}^H\widetilde{\mathbf{x}}] - 2\mathrm{Re}[\mathbf{z}^H\widetilde{\mathbf{x}}] \sim \mathcal{N}(\|\widetilde{\mathbf{x}}\|_2^2 - 2\mathrm{Re}[\mathbf{x}^H\widetilde{\mathbf{x}}], \frac{N_0\|\widetilde{\mathbf{x}}\|_2^2}{|h_n|^2})$. Finally, $\varphi_n \sim \mathcal{N}(\mu_{\varphi_n}, \sigma_{\varphi_n}^2)$, $\mu_{\varphi_n} = (\|\widetilde{\mathbf{x}}\|_2^2 - 2\mathrm{Re}[\mathbf{x}^H\widetilde{\mathbf{x}}])$ and $\sigma_{\varphi_n}^2 = N_0\|\widetilde{\mathbf{x}}\|_2^2$.

B. JMLSD UNION BOUND ANALYSIS

The BER for a given sequence $\mathbf{x}$ can be expressed as $\Pr(\arg\{\varphi_n|\mathbf{x}, \widetilde{\mathbf{x}} = \mathbf{x}\} \neq \arg\min_{\widetilde{\mathbf{x}}}\{\varphi_n|\mathbf{x}, \mathbf{w}_n = 0\})$. However, computing such a probability is prohibitively expensive because of the large number of cases. Hence, we propose an approximation based on PEP, where the union bound on PEP is an upper bound for BER. To compute the PEP, let $\mathbf{x}$ and $\bar{\mathbf{x}}$ be the transmitted and the erroneously decoded sequences with respect to U_n. Therefore,

$$\begin{aligned}\Pr(\mathbf{x} \to \bar{\mathbf{x}}) &= \Pr\left(\left\|\check{\mathbf{r}}_n - |h_n|\bar{\mathbf{x}}\right\|_2^2 < \left\|\check{\mathbf{r}}_n - |h_n|\mathbf{x}\right\|_2^2\right) \\ &= \Pr\left(\mathrm{Re}\left[(\mathbf{x} - \bar{\mathbf{x}})^H\mathbf{w}_n\right] > 0.5|h_n|\|\mathbf{x} - \bar{\mathbf{x}}\|_2^2\right)\end{aligned} \tag{20}$$

where $\mathrm{Re}[(\mathbf{x} - \bar{\mathbf{x}})^H\mathbf{w}_n] \sim \mathcal{N}(0, \sigma_{\bar{w}_n}^2)$ and $\sigma_{\bar{w}_n}^2 = \frac{N_0}{2}\|\mathbf{x} - \bar{\mathbf{x}}\|_2^2$. Therefore,

$$\begin{aligned}\Pr(\mathbf{x} \to \bar{\mathbf{x}}) &= \frac{1}{\sqrt{2\pi\sigma_{\bar{w}_n}^2}}\int_{\frac{|h_n|\|\mathbf{x}-\bar{\mathbf{x}}\|_2^2}{2}}^{\infty} e^{-\frac{\bar{w}_n^2}{2\sigma_{\bar{w}_n}^2}}\, d\bar{w}_n \\ &= Q(0.5\lambda_n\|\mathbf{x} - \bar{\mathbf{x}}\|_2)\end{aligned} \tag{21}$$

where $\lambda_n = \sqrt{\gamma_n}$, $\gamma_n = \frac{2|h_n|^2}{N_0}$. Consequently, the union bound can be written as

$$P_{B_n} \le \frac{1}{|\mathrm{X}|}\sum_{\mathbf{x}\in\chi}\sum_{\bar{\mathbf{x}}\neq\mathbf{x}}\Pr(\mathbf{x} \to \bar{\mathbf{x}}) \tag{22}$$

where $|\mathrm{X}| = M_1^{\tau_1} \times M_2^{\tau_2}$.

IV. MR-SIC DETECTOR BIT ERROR RATE ANALYSIS

This section derives the BER conditioned on γ_n, P_{B_n}. For mathematical tractability, the proposed detector performance is evaluated for the two-user scenario. The analysis considers a wide range of modulations such as BPSK and M_n-QAM where $M_n \in \{4, 16, 64\}$. The conditional BER can be expressed as

$$P_{B_n} = \frac{1}{|\mathrm{X}|}\sum_{i=1}^{|\mathrm{X}|}P_{B_n}^{\mathcal{C}_i} \tag{23}$$

where $P_{B_n}^{\mathcal{C}_i}$ is the BER for the Case-i and $n \in \{1, 2\}$.

A. BER ANALYSIS: FAR USER (U_2)

Because the far user signal is over-sampled by a factor τ_1 and the channel is fixed for a period of T_2, the sum $\mathbf{1}_2^\top\mathbf{r}_n$ in (8) becomes

$$\mathbf{1}_2^\top\mathbf{r}_2 = \sum_{i=1}^{T_2} r_2[i] = \sum_{i=1}^{T_2} h_2x[i] + w_2[i] = h_2\mathbf{1}_2^\top\mathbf{x} + \mathbf{1}_2^\top\mathbf{w}_n \tag{24}$$

where $\mathbf{1}_2^\top\mathbf{x}$ and $\widetilde{w}_2 \triangleq \mathbf{1}_2^\top\mathbf{w}_2$ are the desired signal and AWGN after samples combining, $\widetilde{w}_2 \sim \mathcal{CN}(0, T_2N_0)$, $\mathrm{Re}[\widetilde{w}_2] \triangleq \widetilde{w}_2^i$, $\mathrm{Im}[\widetilde{w}_2] \triangleq \widetilde{w}_2^q$, $\{\widetilde{w}_2^i, \widetilde{w}_2^q\} \sim \mathcal{N}(0, T_2\frac{N_0}{2})$, $A_{\nu_1\nu_2\ldots\nu_N} = \sum_{n=1}^N \nu_n\sqrt{\frac{\alpha_n}{\kappa_n}}$, and, $\grave{\nu}_n \triangleq -\nu_n$. If any of the subscripts has more than one digit, then $A_{\nu_1\nu_2\ldots\nu_N} \to A_{\nu_1,\nu_2,\ldots,\nu_N}$. The normalization factor κ_n is used to ensure that $\mathbb{E}[|x_n[\ell]|^2] = 1$, for a square QAM,

$$\kappa_n \triangleq 2(M_n - 1)/3. \tag{25}$$

It is worth noting that the BER of U_2 in any of the τ_2 samples without combining is identical to SR-NOMA [33, eq. (4)].

To evaluate the BER of U_2, it is necessary to evaluate the impact of the sample combining process on the desired signal, that is $\sum_{i=1}^{\tau_1} x[i] = \tau_1x_2[1] + \sum_{i=1}^{\tau_1} x_1[i]$. Table 1 shows an example for $T_2 \in \{2, 3\}$, $[M_1, M_2] \triangleq \mathbb{m} = [2, 2]$. Moreover, the combining process would result in a new constellation diagram for the desired signal as shown in Fig. 4. As can be seen in Table 1, the output of the

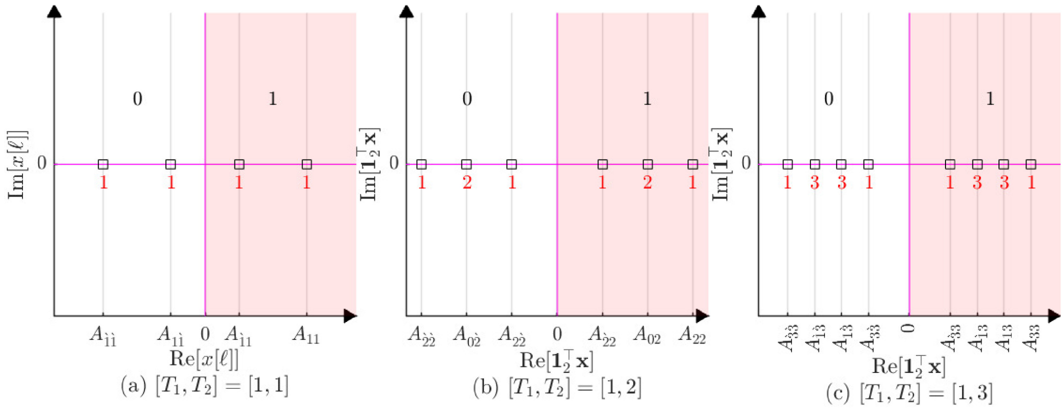

FIGURE 4. Constellation diagrams for U_2 after combining, $\mathrm{m} = [2, 2]$.

TABLE 1. U_2 samples combining outcome for $\mathrm{m} = [2, 2]$, and $T_2 = 2$, $h_n = 1$, $\tau_1 = 2$, and $\mathbf{1}_2 \in \mathbf{1}^{T_2 \times 1}$.

	$\mathbf{x}_1$		$\mathbf{x}_2$		$\mathbf{x}$		
Case	$x_1[1]$	$x_1[2]$	$x_2[1]$	$x_2[2]$	$x[1]$	$x[2]$	$\mathbf{1}_2^\top \mathbf{x}$
1	$\grave{1}$	$\grave{1}$	$\grave{1}$	$\grave{1}$	$A_{\grave{1}\grave{1}}$	$A_{\grave{1}\grave{1}}$	$A_{\grave{2}\grave{2}}$
2	$\grave{1}$	1	$\grave{1}$	$\grave{1}$	$A_{\grave{1}\grave{1}}$	$A_{1\grave{1}}$	$A_{0\grave{2}}$
3	1	$\grave{1}$	$\grave{1}$	$\grave{1}$	$A_{1\grave{1}}$	$A_{\grave{1}\grave{1}}$	$A_{0\grave{2}}$
4	1	1	$\grave{1}$	$\grave{1}$	$A_{1\grave{1}}$	$A_{1\grave{1}}$	$A_{2\grave{2}}$
5	$\grave{1}$	$\grave{1}$	1	1	$A_{\grave{1}1}$	$A_{\grave{1}1}$	$A_{\grave{2}2}$
6	$\grave{1}$	1	1	1	$A_{\grave{1}1}$	A_{11}	A_{02}
7	1	$\grave{1}$	1	1	A_{11}	$A_{\grave{1}1}$	A_{02}
8	1	1	1	1	A_{11}	A_{11}	A_{22}

combining process is not unique where certain outputs are repeated more than once. In Fig. 4, the bits of U_2 are labeled above the x-axis while the number of repetitions of each point is marked below the constellation points.

To derive the BER in the general form, we derive it initially for specific modulation schemes and values of T_2, then the analysis is extended to the general case.

1) $M_1 = M_2 = 2$

The constellation diagrams considering $T_2 \in \{1, 2, 3\}$ are shown in Fig. 4. The figure also shows the decision regions of bit $b_2^{(1)}$. The analysis is done as follows:

- $T_2 = 1$: For this configuration, two cases should be considered:
  $\mathcal{C}_1$: $\mathbf{x} = [A_{\grave{1}1}]$. Therefore,
  $$P_{B_2}^{\mathcal{C}_1} = \Pr\left(\tilde{w}_2^i < -A_{\grave{1}1}\right) = Q\left(A_{\grave{1}1}\lambda_2\right). \tag{26}$$
  $\mathcal{C}_2$: $\mathbf{x} = [A_{11}]$. Therefore,
  $$P_{B_2}^{\mathcal{C}_2} = \Pr\left(\tilde{w}_2^i < -A_{11}\right) = Q(A_{11}\lambda_2). \tag{27}$$
  Consequently,
  $$P_{B_2} = \sum_{i=1}^{2} \frac{P_{B_2}^{\mathcal{C}_i}}{2} = \frac{Q\left(A_{\grave{1}1}\lambda_2\right) + Q(A_{11}\lambda_2)}{2}. \tag{28}$$
- $T_2 = 2$: For this configuration, four cases should be considered, two of which are identical:
  $\mathcal{C}_1$: $\mathbf{x} = [A_{\grave{1}1}, A_{\grave{1}1}]^\top$. Hence, $\mathbf{1}_2^\top \mathbf{x} = A_{\grave{2}2}$. Therefore,
  $$P_{B_2}^{\mathcal{C}_1} = \Pr\left(\tilde{w}_2^i < -A_{\grave{2}2}\right) = Q\left(A_{\grave{2}2}\bar{\lambda}_2\right) \tag{29}$$
  where $\bar{\lambda}_n \triangleq \sqrt{\frac{\gamma_n}{\tau_1}}$.
  $\mathcal{C}_2$ and $\mathcal{C}_3$: $\mathbf{x} = [A_{\grave{1}1}, A_{11}]^\top$ and $\mathbf{x} = [A_{11}, A_{\grave{1}1}]^\top$. Hence, $\mathbf{1}_2^\top \mathbf{x} = A_{02}$. Therefore,
  $$P_{B_2}^{\mathcal{C}_2} = P_{B_2}^{\mathcal{C}_3} = \Pr\left(\tilde{w}_2^i < -A_{02}\right) = Q\left(A_{02}\bar{\lambda}_2\right). \tag{30}$$
  $\mathcal{C}_4$: $\mathbf{x} = [A_{11}, A_{11}]^\top$. Hence, $\mathbf{1}_2^\top \mathbf{x} = A_{22}$. Therefore,
  $$P_{B_2}^{\mathcal{C}_4} = \Pr\left(\tilde{w}_2^i < -A_{22}\right) = Q\left(A_{22}\bar{\lambda}_2\right). \tag{31}$$

Consequently,

$$P_{B_2} = \frac{1}{4}\left(Q\left(A_{\grave{2}2}\bar{\lambda}_2\right) + 2Q\left(A_{02}\bar{\lambda}_2\right) + Q\left(A_{22}\bar{\lambda}_2\right)\right). \tag{32}$$

The configurations for $T_2 = 3$ and 4 can be analyzed following the same approach. By considering all scenarios and observing the patterns for the BER expressions, the generalized BER can be expressed as

$$P_{B_2} = \frac{1}{2^{\tau_1}} \sum_{i=0}^{\tau_1} \binom{\tau_1}{i}_2 Q\left(A_{\nu_i,\tau_1}\bar{\lambda}_2\right) \tag{33}$$

where $\nu_i = (2i - 1)\tau_1$. This expression can be approximated by considering the most-dominant term, which corresponds to the Q function with the minimum argument value, i.e., A_{ν_i,τ_1} is minimized for $i = 0$. Therefore,

$$P_{B_2} \approx \frac{1}{2^{\tau_1}} Q\left(A_{\grave{\tau}_1,\tau_1}\bar{\lambda}_2\right). \tag{34}$$

Consequently, as τ_1 increases, the BER improves because $\frac{1}{2^{\tau_1}}$ decreases and the argument of the Q functions increases.

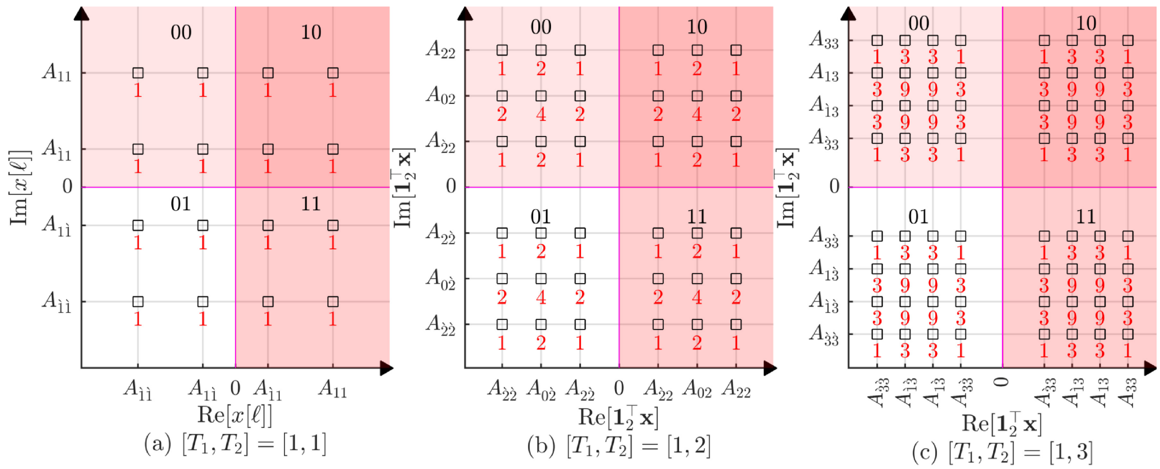

FIGURE 5. The constellation diagram for U_2 after samples combining at the receiver where $\mathfrak{m} = [4, 4]$, the first and second bits of U_2 are shown in black, the number of overlapping symbols is in red: (a) $T_2 = 1$. (b) $T_2 = 2$. (c) $T_2 = 3$.

TABLE 2. BER parameters of U_2 in (35) for $\mathfrak{m} = [2, 2]$ and $[4, 4]$.

T_2	1	2	3	4
β	2	4	8	16
$\mathbf{C}$	$[1, 1]$	$[1, 2, 1]$	$[1, 3, 3, 1]$	$[1, 4, 6, 4, 1]$
$\mathbf{L}$	$[A_{\grave{1}1}, A_{11}]$	$[A_{\grave{2}2}, A_{02}, A_{22}]$	$[A_{\grave{3}3}, A_{\grave{1}3}, A_{13}, A_{33}]$	$[A_{\grave{4}4}, A_{\grave{2}4}, A_{04}, A_{24}, A_{44}]$

2) $M_1 = M_2 = 4$

The constellation diagrams considering $T_2 \in \{1, 2, 3\}$ are given in Fig. 5. The figure shows the decision regions of bits $b_2^{(1)}$ and $b_2^{(2)}$ and the number of cases that represent each symbol. By considering the quadrature phase-shift keying (QPSK) symbol as two orthogonal BPSK symbols, the BER for this case can be expressed using (33) as well. However, it should be noted that $A_{\nu_i \tau_1}$ in (33) depends on M_n due to the normalization factor κ_n in (25). Therefore, the BER expressions for the two cases are different, but they follow the same general structure.

To simplify the evaluation of (33), it can be expressed as

$$P_{B_2} = \frac{1}{\beta} \sum\nolimits_i c_i Q\big(l_i \bar{\lambda}_2\big) \tag{35}$$

where β, l_i and c_i are modulation and symbol rate dependent parameters, which are given in Table 2 for the BPSK and QPSK scenarios. It can be seen from the table that l_i $\forall i$ follows Pascal's triangle, which can also be inferred from the binomial coefficient in (33). For QPSK, it can be seen from the constellation diagrams that the number of horizontal and vertical repetitions is a normalized Pascal triangle. Also, the amplitude expansions in the in-phase or quadrature directions are identical due to the square nature of M_1 and M_2.

3) HIGH ORDER QAM

Following the same approach, the BER parameters for the BER in (35) with $M_n \in \{4, 16, 64\}$ are summarized in Appendix B, Tables 4, 5 and 6. In these tables, the parameters c_i and l_i are obtained from vectors $\mathbf{c}$ and $\boldsymbol{l}$ respectively, where $\mathbf{c} = \mathcal{V}(\mathbf{C}^\top)$, where $\mathcal{V}$ is the matrix vectorization process [34, pp. 118].

By expanding (35) using the derived parameters, P_{B_2} can be expressed as (37) where the probability of error for the kth bit $P_{B_2}^{(k)}$ is given in (38), shown at the bottom of the next page and $\delta_i = (2i - \sqrt{M_1} - 1)\tau_1$ and $\bar{\delta}_m = (2m - 1)\tau_1$. It is worth noting that (38) is also applicable to SR-NOMA where $\tau_1 = 1$. Furthermore, the expression in (38) can be approximated by considering the most-dominant term, that is the Q function with the minimum argument value, i.e., $A_{\delta_i, \bar{\delta}_m}$ is minimized for $i = 0$ and $m = 1$. Therefore,

$$P_{B_2}^{(k)} \approx \frac{2^k Q\Big(A_{(\sqrt{M_1}+1)\grave{\tau}_1, \tau_1} \bar{\lambda}_2\Big)}{\sqrt{M_1^{\tau_1} M_2}}. \tag{36}$$

Consequently, as τ_1 increases, the BER improves because $\frac{2^k}{\sqrt{M_1^{\tau_1} M_2}}$ decreases and the argument of the Q function increases. Finally, the BER for U_2 can be written as

$$P_{B_2} = \frac{1}{\log_2 \sqrt{M_2}} \sum_{k=1}^{\log_2 \sqrt{M_2}} P_{B_2}^{(k)}. \tag{37}$$

B. BER ANALYSIS: NEAR USER (U_1)

The near user should apply SIC to cancel the interference and then use single-user MLD to detect its symbols. Hence, BER depends on the SIC result, which is characterized by P_{B_2}. By noting that, for similar α_1 values, $P_{B_2}|[T_2 > 1] < P_{B_2}|[T_2 = 1]$, then $P_{B_1}|[T_2 > 1] < P_{B_1}|[T_2 = 1]$. Moreover,

TABLE 3. BER parameters of U_1 for $\mathfrak{m} = [2, 2]$.

$T_2 = 1$			$T_2 = 2$			$T_2 = 3$		
C	$\mathcal{F}$	Arg.	**C**	$\mathcal{F}$	Arg.	**C**	$\mathcal{F}$	Arg.
1	$\Psi(\cdot)$	$\{(A_{10})\}$	1	$\Psi(\cdot)$	$\{(A_{10})\}$	1	$\Psi(\cdot)$	$\{(A_{10})\}$
$\frac{1}{2}$	$\Psi(\cdot)$	$\{(A_{\grave{1}1})\}$	$\frac{1}{4}$	$\Psi(\cdot)$	$\left\{\left(\frac{A_{\grave{2}2}}{\sqrt{\tau_1}}\right), \left(\frac{A_{02}}{\sqrt{\tau_1}}\right)\right\}$	$\frac{1}{8}$	$\Psi(\cdot)$	$\left\{\left(\frac{A_{\grave{3}3}}{\sqrt{\tau_1}}\right), 2\left(\frac{A_{\grave{1}3}}{\sqrt{\tau_1}}\right), \left(\frac{A_{13}}{\sqrt{\tau_1}}\right)\right\}$
$\frac{1}{2}$	$\Psi(\cdot)$	$\{(A_{12})\}$	$\frac{1}{4}$	$\Phi(\cdot)$	$\{(A_{12}, A_{02}), (A_{12}, A_{22})\}$	$\frac{1}{8}$	$\Phi(\cdot)$	$\{(A_{12}, A_{\grave{1}3}), 2(A_{12}, A_{13}), (A_{12}, A_{33})\}$
$-\frac{1}{2}$	$\Psi(\cdot)$	$\{(A_{\grave{1}2})\}$	$-\frac{1}{4}$	$\Phi(\cdot)$	$\{(A_{\grave{1}2}, A_{\grave{2}2}), (A_{\grave{1}2}, A_{02})\}$	$-\frac{1}{8}$	$\Phi(\cdot)$	$\{(A_{\grave{1}2}, A_{\grave{3}3}), 2(A_{\grave{1}2}, A_{\grave{1}3}), (A_{\grave{1}2}, A_{13})\}$
$-\frac{1}{2}$	$\Psi(\cdot)$	$\{(A_{11})\}$	$-\frac{1}{4}$	$\Phi(\cdot)$	$\{(A_{10}, A_{\grave{2}2}), 2(A_{10}, A_{02}), (A_{10}, A_{22})\}$	$-\frac{1}{8}$	$\Phi(\cdot)$	$\{(A_{10}, A_{\grave{3}3}), 3(A_{10}, A_{\grave{1}3}), 3(A_{10}, A_{13}), (A_{10}, A_{33})\}$

P_{B_1} is larger than the OMA case, that is, $P_{B_1}|[\alpha_2 = 0, T_1 = 1]$. Consequently, the MR-NOMA BER is bounded by

$$\underbrace{P_{B_1}|[\alpha_2 = 0, T_1 = 1]}_{\text{OMA}} < P_{B_1} < \underbrace{P_{B_1}|[T_1 = T_2 = 1]}_{\text{SR-NOMA}}. \tag{39}$$

While the bounds are valid for any system parameters, their tightness depends on the signal to noise ratio (SNR), T_2, and α_1.

To derive the BER of the MR-NOMA system, three events should be considered, 1) Event A: $\widehat{x}_1[\ell] \neq x_1[\ell]$, 2) B_C: $\widehat{x}_2[\ell] = x_2[\ell]$, and 3) B_I: $\widehat{x}_2[\ell] \neq x_2[\ell]$. Consequently,

$$P_{B_1} = \Pr(B_C, A) + \Pr(B_I, A). \tag{40}$$

Assuming that the signals are real, A and B would be associated with $w_n^i[\ell]$ and $\widetilde{w}_n^i$, respectively. Therefore, the joint PDF should be found. Since $w_n^i[\ell]$ and $\widetilde{w}_n^i$ follow Gaussian distributions, their joint PDF is jointly Gaussian. For notational simplicity, let $y_1 = w_n^i[\ell] \sim \mathcal{N}(0, \frac{N_0}{2})$ and $y_2 = \widetilde{w}_n^i \sim \mathcal{N}(0, T_2\frac{N_0}{2})$. Therefore, the joint PDF of two jointly Gaussian random variables, y_1 and y_2 is given as

$$\begin{aligned} f_{y_1 y_2}(y_1, y_2) &= \frac{\exp\left(\frac{-1}{2\bar{\rho}}\left[\frac{y_1^2}{\sigma_{y_1}^2} + \frac{y_2^2}{\sigma_{y_2}^2} - 2\rho(y_1, y_2)\frac{y_1 y_2}{\sigma_{y_1}\sigma_{y_2}}\right]\right)}{2\pi\sigma_{y_1}\sigma_{y_1}\sqrt{\bar{\rho}}} \\ &= \frac{\exp\left(\frac{-2}{\bar{\rho}N_0}\left[y_1^2 + \frac{1}{T_2}\left(y_2^2 - 2\rho(y_1, y_2)y_1 y_2\right)\right]\right)}{\pi N_0\sqrt{T\bar{\rho}}} \end{aligned} \tag{41}$$

where $\rho(y_1, y_2) = \frac{\text{Cov}(y_1, y_2)}{\sigma_{y_1}\sigma_{y_2}}$ and it is the correlation factor between y_1 and y_2, $\bar{\rho} = (1 - \rho^2(y_1, y_2))$. Such joint PDF is known as an elliptically rotated joint Gaussian distribution. Furthermore, the covariance between y_1 and y_2 can be computed as $\text{Cov}(y_1, y_2)$

$$\begin{aligned} &= \text{Cov}\left(w_n^i[m], \sum\nolimits_m w_n^i[m]\right) \\ &= \text{Cov}\left(w_n^i[m], w_n^i[m]\right) + \sum\nolimits_{m \neq j} \text{Cov}\left(w_n^i[m], w_n^i[j]\right) \\ &= \text{Var}\left(w_n^i[m]\right) = N_0/2. \end{aligned} \tag{42}$$

Consequently, $\rho(y_1, y_2) = \frac{1}{\sqrt{T_2}}$ which indicates a weak correlation. Hence, we can assume independent events. Therefore, $\Pr(A, B) \approx \Pr(A)\Pr(B)$. Following the total probability theory, the conditional BER for a given transmitted sequence can be computed considering the cases $\mathcal{C}_i$ of correct and incorrect SIC detection. Thus,

$$P_{B_1}^{(i)} = \epsilon|\mathcal{C}_i \times (1 - \xi|\mathcal{C}_i) + \varepsilon|\mathcal{C}_i \times \xi|\mathcal{C}_i \tag{43}$$

where $\epsilon|\mathcal{C}_i = \Pr(A_i|B_C)$, $\varepsilon|\mathcal{C}_i = \Pr(A_i|B_I)$, A_i is the event of erroneous detection for a given transmitted sequence, $\xi|\mathcal{C}_i = \Pr(B_I)$ and $1 - \xi|\mathcal{C}_i = \Pr(B_C)$. It should be noted that an incorrect SIC outcome may have $M_2 - 1$ different values. Therefore, analyzing the BER becomes tedious for $M_2 > 2$. Hence, only the case of $\mathfrak{m} = [2, 2]$ is illustrated.

Proposition 1: The BER has the following general form

$$P_{B_1} = \sum\nolimits_{i=1}^{5} c_i \mathcal{F}_i\left(\text{Arg}_i\right) \tag{44}$$

where $\mathcal{F}$ can be either $\Psi(a) \triangleq Q(a\lambda_1)$ or $\Phi(a, b) \triangleq Q(a\lambda_1)Q(b\bar{\lambda}_1)$. Also, we define $\mathcal{F}(\text{Arg}_i, 2\text{Arg}_j, \text{Arg}_k) \triangleq \mathcal{F}(\text{Arg}_i) + 2\mathcal{F}(\text{Arg}_j) + \mathcal{F}(\text{Arg}_k)$. The BER parameters are summarized in Table 3.

Proof: See Appendix C. ■

The BER can be approximated by considering the most-dominant term. From Table 3, the terms that include a product of two Q functions can be ignored as their values are typically negligible. Therefore, the most-dominant term is related to the Q function with the minimum argument, i.e., $A_{\grave{\tau}_1, \tau_1}$. Hence, the BER approximation can be written as

$$P_{B_1} \approx \frac{1}{2^{\tau_1}} Q\left(A_{\grave{\tau}_1, \tau_1}\bar{\lambda}_1\right). \tag{45}$$

Consequently, as τ_1 increases, the BER improves because $\frac{1}{2^{\tau_1}}$ decreases and the argument of the Q function increases.

C. POWER ALLOCATION FOR MR-NOMA

Unlike SR-NOMA, the BER of MR-NOMA depends on both the power allocation factor α_1 and symbol period T_2. The power allocation can be formulated as an optimization problem where the objective is to minimize the BER for

$$P_{B_2}^{(k)} = \sum_{m=1}^{(1-2^{-k})\sqrt{M_2}} \sum_{i=0}^{(\sqrt{M_1}-1)\tau_1} (-1)^{\left\lfloor \frac{2^k(m-1)}{2\sqrt{M_2}} \right\rfloor} \left(2^{k-1} - \left\lfloor \frac{2^k(m-1)}{2\sqrt{M_2}} + \frac{1}{2} \right\rfloor\right) \binom{T_2}{i}_{\sqrt{M_1}} \frac{2Q\left(A_{\delta_i, \bar{\delta}_m}\bar{\lambda}_2\right)}{\sqrt{M_1^{\tau_1} M_2}}. \tag{38}$$

one user while satisfying a predefined BER threshold for the other user. For given $\{\gamma_n, M_n, T_n\}$, $n \in \{1,2\}$, the power allocation process can be formulated as

$$\min_{\alpha_1} \; P_{B_1}(\alpha_1) \tag{46a}$$
$$\text{Subject to:} \; P_{B_2}(\alpha_1) \leq \zeta \tag{46b}$$
$$\alpha_1 < \alpha_{1,\max} \tag{46c}$$

where (46a) is the objective function that is inversely proportional to α_1, γ_1 and T_2. The first constraint in (46b) is used to strictly satisfy the BER threshold ζ of U_2, and constraint (46c) limits the power to the maximum allowed α_1 that ensures reliable SIC detection for both users [28]. Because P_{B_2} monotonically increases and P_{B_1} monotonically decreases versus α_1, then the optimum power α_1^* should be selected so that $P_{B_2}(\alpha_1^*) = \zeta$. Due to the intractability of P_{B_1}, the power allocation is performed using the lower bound in (39), which is relatively accurate at moderate and high SNRs.

Similarly, the optimal power assignment that minimizes P_{B_2} is formulated as

$$\min_{\alpha_1} \; P_{B_2}(\alpha_1) \tag{47a}$$
$$\text{Subject to:} \; P_{B_1}(\alpha_1) \leq \zeta \tag{47b}$$
$$\alpha_1 < \alpha_{1,\max} \tag{47c}$$

and the optimum power allocation can be obtained so that $P_{B_1}(\alpha_1^*) = \zeta$. Solving the power optimization problem for NOMA analytically is generally infeasible due to the high complexity and nonlinearity of the BER expressions [2]. Hence in this work, the optimization problem is solved numerically. Moreover, for MR-NOMA, the P_{B_1} expression is intractable, and hence it is approximated by the lower bound in (39).

V. NUMERICAL RESULTS AND DISCUSSIONS

This section compares the two-user BER results of the MR-NOMA with the SR-NOMA, where the latter is denoted by $[T_1, T_2] = [1, 1]$. The analytical BER for JMLSD and the proposed low-complexity MR-SIC are computed using the expressions derived in Sections III and IV, while the analytical BER of the benchmark is computed based on [27]. The BER is validated using Monte Carlo simulation with 10^5 realizations. Throughout the section, the markers represent the simulation results, whereas the lines represent the analytical results. In addition, the optimal power allocation that minimizes either user's BER and strictly satisfy the other's QoS requirements are computed. While assuming $h_n = 1\,\forall n$, the SNR is defined as $\text{SNR} \triangleq \frac{1}{N_0}$, where N_0 is common for both users. Unless otherwise stated, $\alpha_1 = \frac{M_1-1}{M_1M_2-1}$ [33]. Also α_1 is bounded by $0 < \alpha_1 < \alpha_{1,\max}$ to allow reliable SIC detection, where $\alpha_{1,\max} = \frac{\kappa_1}{\kappa_1+\kappa_2\Lambda_1^2}$ and $\Lambda_n = \sqrt{M_n} - 1$ for square QAM [27]. The performance of MR-NOMA using JMLSD and MR-SIC detectors is compared to the SR-NOMA where $T_2 = 1$ in the presented results.

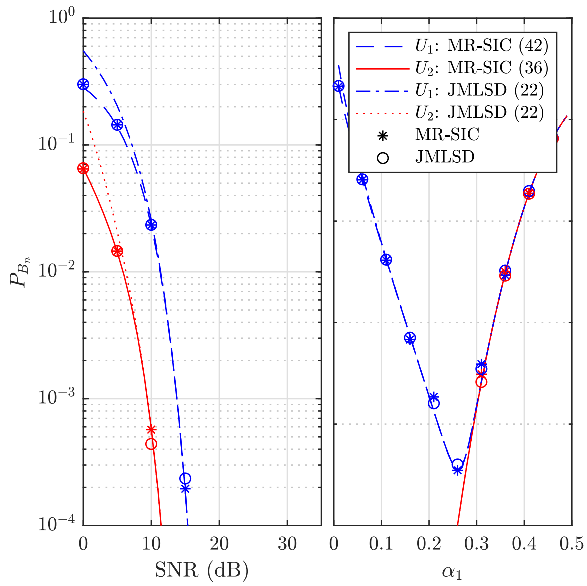

FIGURE 6. BER performance comparison between JMLSD and SIC detectors, where $\mathfrak{m} = [2, 2]$ and $T_2 = 2$: (left) $[\alpha_1, \alpha_2] = [0.2, 0.8]$. (right) SNR = 15 dB.

Fig. 6 compares the BER of JMLSD and MR-SIC assuming BPSK for both users and $T_2 = 2$. It can be seen that the analytical and simulation results match closely, which is also the case in the subsequent figures. Furthermore, both detectors provide identical performance, which is due to the fact that MR-SIC is an optimal low complexity implementation of the JMLSD. Also, the derived bound for the JMLSD in (22) is seen to be tight in low SNR regime while it matches the exact performance in the moderate and high SNR regimes.

Fig. 7 shows P_{B_1} versus α_1 where SNR = 15 dB. Unlike the lower bound, which monotonically decreases, the MR-NOMA behavior is similar to that of SR-NOMA with $T_2 = 1$. That is, the BER of both is convex with global minima at α_1^*. It can be seen that as T_2 increases, P_{B_1} improves at the expense of the spectral efficiency. This is because the reliability of the SIC process improves as P_{B_2} decreases. In addition, α_1^* shifts towards larger values as T_2 increases. The reason is that the P_{B_2} value that minimizes P_{B_1} can be achieved at lower values of α_2 by increasing the symbol energy of U_2, that is, increasing T_2. Consequently, the excess power allocation factor of U_2 can be allocated to U_1. Furthermore, for $\alpha_1 < \alpha_1^*$, the analytical performance and the lower bound becomes close, indicating that the SIC error is negligible.

Fig. 8 shows the far user BER versus α_1 considering BPSK for both users and various symbol rates, where SNR is 15 dB for $T_2 = 1$ and as T_2 doubles, the SNR is reduced by 3 dB to ensure fair comparison and maintain normalized energy per bit at the receiver end. It is observed that the far user BER increases monotonically versus α_1, while it decreases monotonically versus T_2 at the expense of reduced spectral efficiency. In addition, at

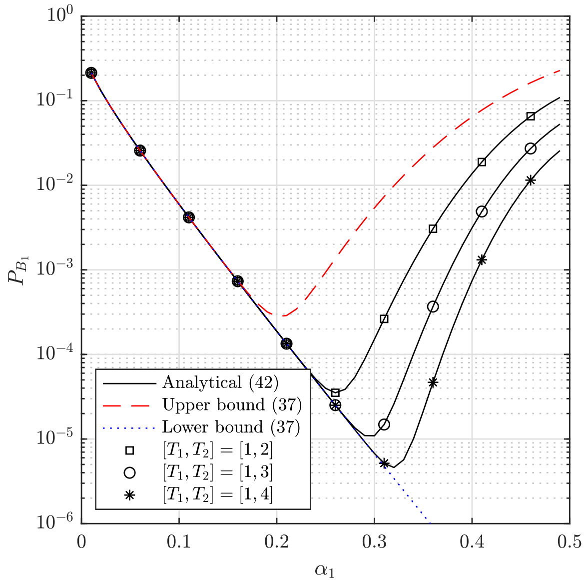

FIGURE 7. Near user BER performance for SIC detector considering various symbol rates, where $\mathfrak{m} = [2, 2]$ and SNR = 15 dB.

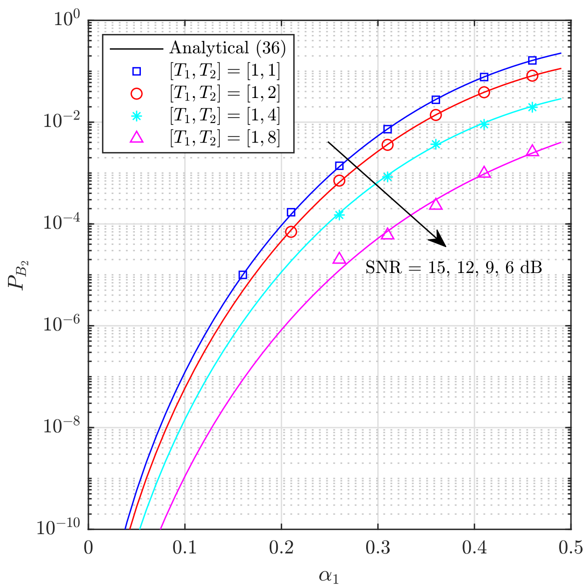

FIGURE 8. Far user BER performance for SIC detector considering various symbol rates, where $\mathfrak{m} = [2, 2]$ and SNR = 15,12,9,6 dB.

low α_1 values, the MR-NOMA performance gain is small. Nonetheless, as $\alpha_1 \to \alpha_{1,\max}$, the MR-NOMA performance gain improves significantly and reaches two orders of magnitude at $\alpha_1 = 0.2$.

Fig. 9 shows the far user BER versus SNR considering identical modulation order for both users and with various symbol rates. It can be seen that to achieve a fixed BER threshold, higher SNR levels are required as M_n increases. For instance, while fixing $T_2 = 1$ and considering BPSK as a benchmark, QPSK requires extra 3 dB to achieve a BER of 10^{-2}, whereas 16-QAM and 64-QAM require 13.2 and 21.8 dB, respectively. Furthermore, the MR-NOMA performance gain can be quantified for fixed modulation orders as follows. First, doubling T_2 every time leads to a 3 dB processing gain because the energy collected at the receiver after processing doubles as well. Secondly, while keeping T_2 to be even, the interference from the near user signal can be partially canceled. Such a phenomenon leads to a gain, we call it weak-interference cancellation gain, which keeps increasing as M_n increase and it can be quantified as follows. The BPSK/QPSK case gain increases from 1.4–4.2 dB as T_2 increases from 2–8. Similarly, 16-QAM and 64-QAM gain 4.2–8.4 dB and 7.3–11.4 dB, respectively. Moreover, while keeping the bit rate fixed, MR-NOMA shows a performance gain. For example, for a bit rate of 1 bps/Hz, the QPSK case (with $T_2 = 2$) outperforms the BPSK case (with $T_2 = 1$) by 1.4 dB. Similarly, for a bit rate of 0.5 bps/Hz, the QPSK case (with $T_2 = 4$) outperforms the BPSK case (with $T_2 = 2$) by 1.8 dB. Also, for a bit rate of 0.25 bps/Hz, the QPSK case (with $T_2 = 8$) outperforms the BPSK case (with $T_2 = 4$) by 1 dB. In some other scenarios, MR-NOMA shows a performance degradation when the bit rate is fixed. For example, for a bit rate of 2 bps/Hz, the 16-QAM case (with $T_2 = 2$) fall behind the QPSK case (with $T_2 = 1$) by 3 dB.

Fig. 10 shows the far user BER versus SNR considering different modulation orders for both users and various symbol rates, where $M_n \in \{4, 16, 64\}$. The weak-interference cancellation gain can be quantified as follows. The gain for $\mathfrak{m} = [4, 16]$ and $\mathfrak{m} = [4, 64]$ increases from 1.5–4.1 dB as T_2 increases from 2–8. Similarly, $\mathfrak{m} = [16, 4]$ and $\mathfrak{m} = [16, 64]$ gain 3.9–8.5 dB and 4.4–8.1 dB, respectively. In addition, $\mathfrak{m} = [64, 4]$ and $\mathfrak{m} = [64, 16]$ gain 7.3–12.6 dB and 7.5–12.1 dB, respectively. Furthermore, while fixing the modulation order of the near user to 64-QAM and the bit rate of the far user to 1 bps/Hz, the $\mathfrak{m} = [64, 16]$ case (with $T_2 = 4$) outperforms the $\mathfrak{m} = [64, 4]$ case (with $T_2 = 2$) by 1.6 dB.

Finally, the power allocation results versus T_2 are shown in Fig. 11, where $\zeta = 10^{-2}$ and the considered pairs of $\mathfrak{m}$ are [4, 4], [16, 4] and [64, 4], and the corresponding γ_1 is 16, 19 and 28 dB, while $\gamma_2 = 8$ dB. Fig. 11a shows α_1^* for (46a) and (47a). It can be seen that α_1^* for (47a) is independent of T_2 because the BER lower bound in (39) is independent of T_2. For α_1^* in (46a), it increases as T_2 increases before it saturates at $\alpha_{1,\max}$. This is because increasing T_2 will decrease P_{B_2} for the same values of α_1. However, as U_2 should achieve $P_{B_2} = \zeta$, α_2 can be reduced and α_1 can be increased to minimize P_{B_1}. On the other hand, Fig. 11b shows the BER performance at the optimal α_1. It can be seen that $P_{B_1}(\alpha_1^*)$ for (47a) is always satisfied at the specified ζ, where it is independent of T_2 because the $P_{B_1}(\alpha_1)$ lower bound in (39) is independent of T_2. Additionally, $P_{B_2}(\alpha_1^*)$ for (47a) continues to improve as T_2 increases because the objective is to minimize $P_{B_2}(\alpha_1)$. Furthermore, $P_{B_1}(\alpha_1^*)$ for (46a) continues to improve as T_2 increases before it saturates, due to the fact that while $P_{B_1}(\alpha_1^*)$ is inversely proportional to α_1^*, the latter

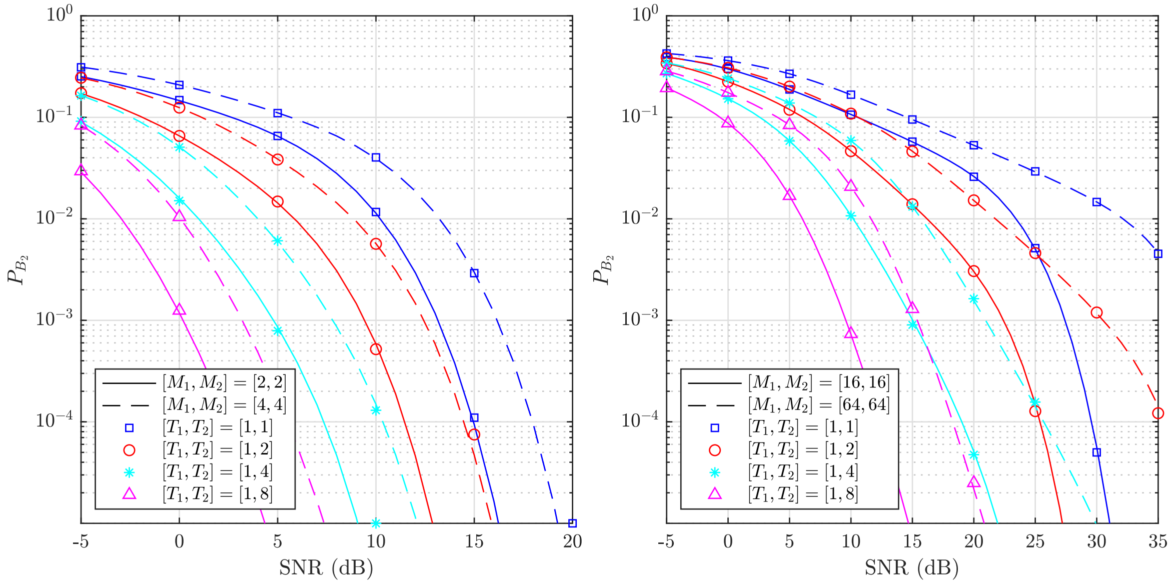

(a) $M_n \in \{2, 4\}$

(b) $M_n \in \{16, 64\}$

FIGURE 9. BER performance for SIC detector considering identical modulation orders where $M_n \in \{2, 4, 16, 64\}$ and $T_2 \in \{1, 2, 4, 8\}$.

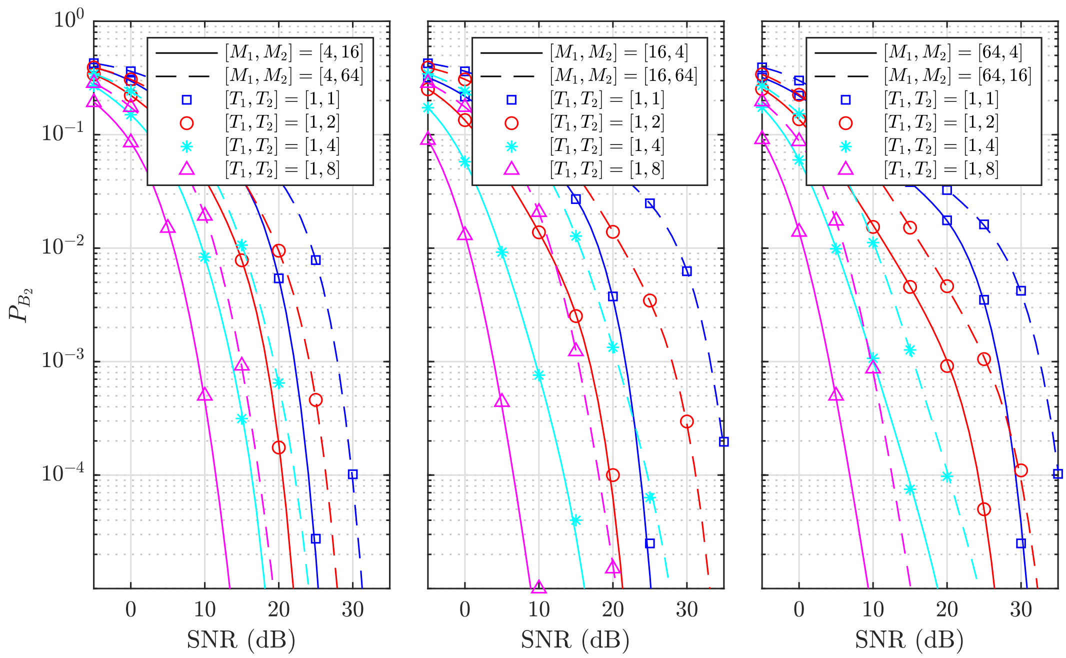

FIGURE 10. BER performance for SIC detector considering non-identical modulation orders where $M_n \in \{4, 16, 64\}$ and $T_2 \in \{1, 2, 4, 8\}$.

continues to increase as T_2 increases before it saturates. Furthermore, $P_{B_2}(\alpha_1^*)$ for (46a) is strictly satisfied up to a certain T_2 value, after which $P_{B_2}(\alpha_1^*)$ becomes less than ζ.

VI. CONCLUSION

To conclude, this work proposes a low-complexity MR-SIC detector for the MR-NOMA system and derives closed-form BER expressions for various modulation orders that are applicable to both SR- and MR-NOMA systems. It was shown that MR-NOMA enjoys an additional degree of freedom compared to SR-NOMA, which is the energy dimension. This allows it to improve the BER performance up to two orders of magnitude in certain scenarios, which can be justified by the processing gain and the weak-interference cancellation gain that are exclusive to MR-NOMA. Furthermore, it was demonstrated that MR-NOMA provides a more granular resolution to achieve a wider range of bit rate requirements per user by varying the symbol duration of the low-rate user.

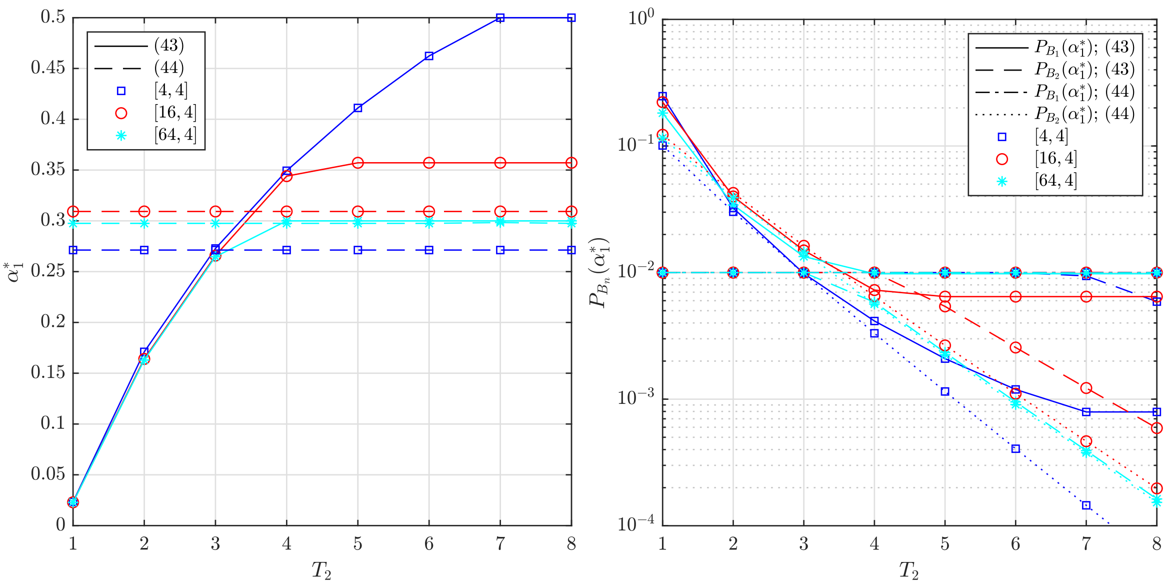

(a) Optimal power assignment (b) Optimal BER performance

FIGURE 11. Optimization results for SIC detector where $\zeta = 10^{-2}$, $\gamma_1 \in \{16, 19, 28\}$ dB, $\gamma_2 = 8$ dB, $M_1 \in \{4, 16, 64\}$ and $M_2 = 4$.

Future work on this topic will focus on uplink MR-NOMA design and analysis as well as extensions to arbitrary numbers of users. Moreover, the system model can be generalized to cases where low-rate users are the near users, or a hybrid case where users are randomly distributed in a given BS coverage region. It will also evaluate the system performance when multiple antennas are deployed in BS, user devices, or both.

APPENDIX A
MR-SIC AND JMLSD PROOF OF EQUIVALENCE

To facilitate the proof, let $N = 2$. Hence, the JMLSD expressed in (7) can be simplified to

$$\begin{aligned}\{\widehat{\mathbf{x}}_1, \widehat{\mathbf{x}}_2\} &= \arg\min_{\widetilde{\mathbf{x}}} \|\mathbf{r}_n - h_n \widetilde{\mathbf{x}}\|_2^2 \\ &= \arg\min_{\widetilde{\mathbf{x}}} |h_n|^2 \|\widetilde{\mathbf{x}}\|_2^2 - 2\mathrm{Re}\left[\mathbf{r}_n^H \widetilde{\mathbf{x}}\right]. \end{aligned} \tag{48}$$

Now, considering the low-rate user detection, while noting that $\widehat{x}_2[1] = \widehat{x}_2[2] = \cdots = \widehat{x}_2[T_2] = \widehat{x}_2$, the detector in (48) can be written as

$$\widehat{x}_2 = \arg\min_{\widetilde{x}_2} \left\| \mathbf{r}_n - h_n \sqrt{\alpha_2} \widetilde{x}_2 \mathbf{1}_2 \right\|_2^2 \tag{49}$$

which can be further expanded and simplified as

$$\begin{aligned}\widehat{x}_2 = \arg\min_{\widetilde{x}_2} \Bigg\{ & T_2 \alpha_2 |h_n|^2 |\widetilde{x}_2|^2 \\ & - 2\sqrt{\alpha_2} \mathrm{Re}\left[\left(\sum_{\ell=1}^{T_2} r_n^*[\ell] \right) h_n \widetilde{x}_2 \right] \Bigg\}. \end{aligned} \tag{50}$$

On the other hand, the first step of the MR-SIC detector expressed in (8) can be written for $N = 2$ as

$$\widehat{x}_2 = \arg\min_{\widetilde{x}_2} \left| \sum_{\ell=1}^{T_2} r_n[\ell] - h_n \sqrt{\alpha_2} T_2 \widetilde{x}_2 \right|^2 \tag{51}$$

which can be further expanded and simplified as

$$\begin{aligned}\widehat{x}_2 = \arg\min_{\widetilde{x}_2} \Bigg\{ & T_2^2 \alpha_2 |h_n|^2 |\widetilde{x}_2|^2 \\ & - 2T_2 \sqrt{\alpha_2} \mathrm{Re}\left[\left(\sum_{\ell=1}^{T_2} r_n^*[\ell] \right) h_n \widetilde{x}_2 \right] \Bigg\}. \end{aligned} \tag{52}$$

By noting that T_2 can be taken as a common factor from the two terms, it can be dropped. Hence, the expression in (52) becomes identical to (50). Since the detection of $\widehat{x}_2$ is equivalent in both detectors, therefore, the detection of $\widehat{x}_1[\ell]$ in the following steps is equivalent too. By induction, the proof can be expanded to higher N values.

APPENDIX B
BER PARAMETERS OF FAR USER FOR $M_N \in \{4, 16, 64\}$

The BER parameters for U_2 where $M_n \in \{4, 16, 64\}$, and $T_2 \in \{1, 2\}$ are given in Tables 4, 5, and 6.

APPENDIX C
NEAR USER BER PROOF

This appendix illustrates the proof of BER for $\mathfrak{m} = [2, 2]$.

TABLE 4. BER parameters of U_2 in (35) for $M_1 = 4$. $\mathbf{D}_{a_1,\ldots,a_N}$ is a diagonal matrix whose diagonal elements are the subscripts, $\mathbf{O}_a$ is an $a \times 2$ matrix with ones in all entries, $\mathbf{G}_a$ is an $a \times 3$ matrix where each row has the elements [1, 2, 1].

		$T_2 = 1$			$T_2 = 2$		
$\mathfrak{m}$	$b_2^{(k)}$	**L**	**C**	β	**L**	**C**	β
$[4, 4]$	$b_2^{(1)}$	$\mathbf{A}_1 = [A_{\grave{1}1}, A_{11}]$	$\mathbf{O}_1 = [1, 1]$	2	$\mathbf{Q}_1 = [A_{\grave{2}2}, A_{02}, A_{22}]$	$\mathbf{G}_1 = [1, 2, 1]$	4
$[4, 16]$	$b_2^{(1)}$	$\mathbf{A}_2 = \begin{bmatrix} \mathbf{A}_1 \\ A_{\grave{1}3}, A_{13} \end{bmatrix}$	$\mathbf{D}_{\{1,1\}}\ \mathbf{O}_2$	4	$\mathbf{Q}_2 = \begin{bmatrix} \mathbf{Q}_1 \\ A_{\grave{2}6}, A_{06}, A_{26} \end{bmatrix}$	$\mathbf{D}_{\{1,1\}}\mathbf{G}_2$	8
$[4, 16]$	$b_2^{(2)}$	$\mathbf{A}_3 = \begin{bmatrix} \mathbf{A}_2 \\ A_{\grave{1}5}, A_{15} \end{bmatrix}$	$\mathbf{D}_{\{2,1,\grave{1}\}}\mathbf{O}_3$	4	$\mathbf{Q}_3 = \begin{bmatrix} \mathbf{Q}_2 \\ A_{\grave{2},10}, A_{0,10}, A_{2,10} \end{bmatrix}$	$\mathbf{D}_{\{2,1,\grave{1}\}}\mathbf{G}_3$	8
$[4, 64]$	$b_2^{(1)}$	$\mathbf{A}_4 = \begin{bmatrix} \mathbf{A}_3 \\ A_{\grave{1}7}, A_{17} \end{bmatrix}$	$\mathbf{D}_{\{1,1,1.1\}}\mathbf{O}_4$	8	$\mathbf{Q}_4 = \begin{bmatrix} \mathbf{Q}_3 \\ A_{\grave{2},14}, A_{0,14}, A_{2,14} \end{bmatrix}$	$\mathbf{D}_{\{1,1,1.1\}}\mathbf{G}_4$	16
$[4, 64]$	$b_2^{(2)}$	$\mathbf{A}_6 = \begin{bmatrix} \mathbf{A}_4 \\ \mathbf{A}_{\grave{1}9}, A_{19} \\ A_{\grave{1},11}, A_{1,11} \end{bmatrix}$	$\mathbf{D}_{\{2,2,1,1,\grave{1},\grave{1}\}}\mathbf{O}_6$	8	$\mathbf{Q}_6 = \begin{bmatrix} \mathbf{Q}_5 \\ A_{\grave{2},18}, A_{0,18}, A_{2,18} \\ A_{\grave{2},22}, A_{0,22}, A_{2,22} \end{bmatrix}$	$\mathbf{D}_{\{2,2,1,1,\grave{1},\grave{1}\}}\mathbf{G}_6$	16
$[4, 64]$	$b_2^{(3)}$	$\mathbf{A}_7 = \begin{bmatrix} \mathbf{A}_6 \\ A_{\grave{1},13}, A_{1,13} \end{bmatrix}$	$\mathbf{D}_{\{4,3,\grave{3},\grave{2},2,1,\grave{1}\}}\mathbf{O}_7$	8	$\mathbf{Q}_7 = \begin{bmatrix} \mathbf{Q}_6 \\ A_{\grave{2},26}, A_{0,26}, A_{2,26} \end{bmatrix}$	$\mathbf{D}_{\{4,3,\grave{3},\grave{2},2,1,\grave{1}\}}\mathbf{G}_7$	16

TABLE 5. BER parameters of U_2 in (35) for $M_1 = 16$. $\mathbf{D}_{a_1,\ldots,a_N}$ is a diagonal matrix whose diagonal elements are the subscripts, $\mathbf{O}_a$ is an $a \times 4$ matrix with ones in all entries, $\mathbf{G}_a$ is an $a \times 7$ matrix where each row is equal to $\mathbf{G}_1$.

		$T_2 = 1$			$T_2 = 2$		
$\mathfrak{m}$	$b_2^{(k)}$	**L**	**C**	β	**L**	**C**	β
$[16, 4]$	$b_2^{(1)}$	$\mathbf{A}_1 = [A_{\grave{3}1}, A_{\grave{1}1}, A_{11}, A_{31}]$	$\mathbf{O}_1 = [1, 1, 1, 1]$	4	$\mathbf{Q}_1 = [A_{\grave{6}2}, A_{\grave{4}2}, \ldots, A_{42}, A_{62}]$	$\mathbf{G}_1 = [1, 2, 3, 4, 3, 2, 1]$	16
$[16, 16]$	$b_2^{(1)}$	$\mathbf{A}_2 = \begin{bmatrix} \mathbf{A}_1 \\ A_{\grave{3}3}, A_{\grave{1}3}, A_{13}, A_{33} \end{bmatrix}$	$\mathbf{D}_{\{1,1\}}\ \mathbf{O}_2$	8	$\mathbf{Q}_2 = \begin{bmatrix} \mathbf{Q}_1 \\ A_{\grave{6}6}, A_{\grave{4}6}, \ldots, A_{46}, A_{66} \end{bmatrix}$	$\mathbf{D}_{\{1,1\}}\mathbf{G}_2$	32
$[16, 16]$	$b_2^{(2)}$	$\mathbf{A}_3 = \begin{bmatrix} \mathbf{A}_2 \\ A_{\grave{3}5}, A_{\grave{1}5}, A_{15}, A_{35} \end{bmatrix}$	$\mathbf{D}_{\{2,1,\grave{1}\}}\mathbf{O}_3$	8	$\mathbf{Q}_3 = \begin{bmatrix} \mathbf{Q}_2 \\ A_{\grave{6},10}, A_{\grave{4},10}, \ldots, A_{4,10}, A_{6,10} \end{bmatrix}$	$\mathbf{D}_{\{2,1,\grave{1}\}}\mathbf{G}_3$	32
$[16, 64]$	$b_2^{(1)}$	$\mathbf{A}_4 = \begin{bmatrix} \mathbf{A}_3 \\ A_{\grave{3}7}, A_{\grave{1}7}, A_{17}, A_{37} \end{bmatrix}$	$\mathbf{D}_{\{1,1,1.1\}}\mathbf{O}_4$	16	$\mathbf{Q}_4 = \begin{bmatrix} \mathbf{Q}_3 \\ A_{\grave{6},14}, A_{\grave{4},14}, \ldots, A_{4,14}, A_{6,14} \end{bmatrix}$	$\mathbf{D}_{\{1,1,1.1\}}\mathbf{G}_4$	64
$[16, 64]$	$b_2^{(2)}$	$\mathbf{A}_6 = \begin{bmatrix} \mathbf{A}_4 \\ A_{\grave{3}9}, A_{\grave{1}9}, A_{19}, A_{39} \\ A_{\grave{3},11}, A_{\grave{1},11}, A_{1,11}, A_{3,11} \end{bmatrix}$	$\mathbf{D}_{\{2,2,1,1,\grave{1},\grave{1}\}}\mathbf{O}_6$	16	$\mathbf{Q}_6 = \begin{bmatrix} \mathbf{Q}_4 \\ A_{\grave{6},18}, A_{\grave{4},18}, \ldots, A_{4,18}, A_{6,18} \\ A_{\grave{6},22}, A_{\grave{4},22}, \ldots, A_{4,22}, A_{6,22} \end{bmatrix}$	$\mathbf{D}_{\{2,2,1,1,\grave{1},\grave{1}\}}\mathbf{G}_6$	64
$[16, 64]$	$b_2^{(3)}$	$\mathbf{A}_7 = \begin{bmatrix} \mathbf{A}_6 \\ A_{\grave{3},13}, A_{\grave{1},13}, A_{1,13}, A_{3,13} \end{bmatrix}$	$\mathbf{D}_{\{4,3,\grave{3},\grave{2},2,1,\grave{1}\}}\mathbf{O}_7$	16	$\mathbf{Q}_7 = \begin{bmatrix} \mathbf{Q}_6 \\ A_{\grave{6},26}, A_{\grave{4},26}, \ldots, A_{4,26}, A_{6,26} \end{bmatrix}$	$\mathbf{D}_{\{4,3,\grave{3},\grave{2},2,1,\grave{1}\}}\mathbf{G}_7$	64

TABLE 6. BER parameters of U_2 in (35) for $M_1 = 64$. $\mathbf{D}_{a_1,\ldots,a_N}$ is a diagonal matrix whose diagonal elements are the subscripts, $\mathbf{O}_a$ is an $a \times 8$ matrix with ones in all entries, $\mathbf{G}_a$ is an $a \times 15$ matrix where each row is equal to $\mathbf{G}_1$.

		$T_2 = 1$			$T_2 = 2$		
$\mathfrak{m}$	$b_2^{(k)}$	**L**	**C**	β	**L**	**C**	β
$[64, 4]$	$b_2^{(1)}$	$\mathbf{A}_1 = [A_{\grave{7}1}, A_{\grave{5}1}, \ldots, A_{51}, A_{71}]$	$\mathbf{O}_1 = [1, 1, 1, 1, 1, 1, 1, 1]$	8	$\mathbf{Q}_1 = [A_{\grave{1}4,2}, A_{\grave{1}2,2}, \ldots, A_{12,2}, A_{14,2}]$	$\mathbf{G}_1 = [1, 2, 3, \ldots, 7, 8, 7, \ldots, 3, 2, 1]$	64
$[64, 16]$	$b_2^{(1)}$	$\mathbf{A}_2 = \begin{bmatrix} \mathbf{A}_1 \\ A_{\grave{7}3}, A_{\grave{5}3}, \ldots, A_{53}, A_{73} \end{bmatrix}$	$\mathbf{D}_{\{1,1\}}\ \mathbf{O}_2$	16	$\mathbf{Q}_2 = \begin{bmatrix} \mathbf{Q}_1 \\ A_{\grave{1}4,6}, A_{\grave{1}2,6}, \ldots, A_{12,6}, A_{14,6} \end{bmatrix}$	$\mathbf{D}_{\{1,1\}}\ \mathbf{G}_2$	128
$[64, 16]$	$b_2^{(2)}$	$\mathbf{A}_3 = \begin{bmatrix} \mathbf{A}_2 \\ A_{\grave{7}5}, A_{\grave{5}5}, \ldots, A_{55}, A_{75} \end{bmatrix}$	$\mathbf{D}_{\{2,1,\grave{1}\}}\mathbf{O}_3$	16	$\mathbf{Q}_3 = \begin{bmatrix} \mathbf{Q}_2 \\ A_{\grave{1}4,10}, A_{\grave{1}2,10}, \ldots, A_{12,10}, A_{14,10} \end{bmatrix}$	$\mathbf{D}_{\{2,1,\grave{1}\}}\mathbf{G}_3$	128

A. $T_2 = 1$

$\mathcal{C}_1$: $\mathbf{x} = [A_{\grave{1}1}]$. The error occurs in two ways. First, when SIC is correct, the detected amplitude is $A_{\grave{1}0}$ and the probability of error is

$$P_{B_1}^{\mathcal{C}_{1a}} = \Pr\Big(w_1^i[\ell] > A_{10} \cap w_1^i[\ell] > -A_{\grave{1}1}\Big) = \Pr\Big(w_1^i[\ell] > A_{10}\Big) = Q(A_{10}\lambda_1) \tag{53}$$

whereas when SIC is incorrect, the detected amplitude is $A_{\grave{1}2}$ and the probability of error can be written as

$$P_{B_1}^{\mathcal{C}_{1b}} = \Pr\Big(w_1^i[\ell] > -A_{\grave{1}2} \cap w_1^i[\ell] < -A_{\grave{1}1}\Big) = \Pr\Big(A_{\grave{1}1} < w_1^i[\ell] < A_{\grave{1}2}\Big) = Q\big(A_{\grave{1}1}\lambda_1\big) - Q\big(A_{\grave{1}2}\lambda_1\big). \tag{54}$$

Hence,

$$P_{B_1}^{\mathcal{C}_1} = Q(A_{10}\lambda_1) + Q\big(A_{\grave{1}1}\lambda_1\big) - Q\big(A_{\grave{1}2}\lambda_1\big). \tag{55}$$

$\mathcal{C}_2$: $\mathbf{x} = [A_{11}]$. The error occurs in two ways. First, when SIC is correct, the detected amplitude is A_{10} and the probability of error is

$$P_{B_1}^{\mathcal{C}_{2a}} = \Pr\Big(w_1^i[\ell] < -A_{10} \cap w_1^i[\ell] > -A_{11}\Big) = \Pr\Big(-A_{11} < w_1^i[\ell] < -A_{10}\Big)$$

$$= Q(A_{10}\lambda_1) - Q(A_{11}\lambda_1) \tag{56}$$

whereas when SIC is incorrect, the detected amplitude is A_{12} and the probability of error can be written as

$$\begin{aligned} P_{B_1}^{\mathcal{C}_{2b}} &= \Pr\Big(w_1^i[\ell] < -A_{12} \cap w_1^i[\ell] < -A_{11}\Big) \\ &= \Pr\Big(w_1^i[\ell] < -A_{12}\Big) = Q(A_{12}\lambda_1). \end{aligned} \tag{57}$$

Hence,

$$P_{B_1}^{\mathcal{C}_2} = Q(A_{10}\lambda_1) + Q(A_{12}\lambda_1) - Q(A_{11}\lambda_1). \tag{58}$$

Consequently,

$$P_{B_1} = Q(A_{10}\lambda_1) + \sum_{i \in \{1,\grave{1}\}} \frac{-i}{2} Q(A_{i1}\lambda_1) + \frac{i}{2} Q(A_{i2}\lambda_1). \tag{59}$$

B. $T_2 = 2$

$\mathcal{C}_1$: $\mathbf{x} = [A_{\grave{1}1}, A_{\grave{1}1}]$.

The probability of SIC error can be written as

$$\xi|\mathcal{C}_1 = \Pr(\tilde{w}_1 < -A_{\grave{2}2}) = Q\big(A_{\grave{2}2}\bar{\lambda}_1\big). \tag{60}$$

Hence, $\epsilon|\mathcal{C}_1$ and $\varepsilon|\mathcal{C}_1$ are respectively given by

$$\begin{aligned} \epsilon|\mathcal{C}_1 &= \frac{1}{2}\Pr(w_1[1] > A_{10} \cup w_1[2] > A_{10}) \\ &= Q(A_{10}\lambda_1) \end{aligned} \tag{61}$$

$$\begin{aligned} \varepsilon|\mathcal{C}_1 &= \frac{1}{2}\Pr\big(w_1[1] > -A_{\grave{1}2} \cup w_1[2] > -A_{\grave{1}2}\big) \\ &= \big[1 - Q\big(A_{\grave{1}2}\lambda_1\big)\big]. \end{aligned} \tag{62}$$

Consequently,

$$\begin{aligned} P_{B_1}^{\mathcal{C}_1} &= Q(A_{10}\lambda_1) + Q\big(A_{\grave{2}2}\bar{\lambda}_1\big) - Q\big(A_{\grave{2}2}\bar{\lambda}_1\big) \\ &\quad \times Q(A_{10}\lambda_1) - Q\big(A_{\grave{2}2}\bar{\lambda}_1\big) Q\big(A_{\grave{1}2}\lambda_1\big). \end{aligned} \tag{63}$$

$\mathcal{C}_2$: $\mathbf{x} = [A_{\grave{1}1}, A_{11}]$.

The probability of SIC error can be written as

$$\xi|\mathcal{C}_2 = \Pr(\tilde{w}_1 < -A_{02}) = Q\big(A_{02}\bar{\lambda}_1\big). \tag{64}$$

Hence,

$$\begin{aligned} \epsilon|\mathcal{C}_2 &= \frac{1}{2}\Pr(w_1[1] > A_{10} \cup w_1[2] < -A_{10}) \\ &= Q(A_{10}\lambda_1) \end{aligned} \tag{65}$$

$$\begin{aligned} \varepsilon|\mathcal{C}_2 &= \frac{1}{2}\Pr\big(w_1[1] > -A_{\grave{1}2} \cup w_1[2] < -A_{12}\big) \\ &= \frac{1}{2}\big[1 - Q\big(A_{\grave{1}2}\lambda_1\big) + Q(A_{12}\lambda_1)\big]. \end{aligned} \tag{66}$$

Consequently,

$$\begin{aligned} P_{B_1}^{\mathcal{C}_2} &= Q(A_{10}\lambda_1) + \frac{1}{2} Q\big(A_{02}\bar{\lambda}_1\big) \\ &\quad \times \left[1 - 2Q(A_{10}\lambda_1) + \sum_{i \in \{1,\grave{1}\}} iQ(A_{i2}\lambda_1)\right]. \end{aligned} \tag{67}$$

$\mathcal{C}_3$: $\mathbf{x} = [A_{11}, A_{\grave{1}1}]$ has identical results as $\mathcal{C}_2$.

$\mathcal{C}_4$: $\mathbf{x} = [A_{11}, A_{11}]$.

The probability of SIC error can be written as

$$\xi|\mathcal{C}_4 = \Pr(\tilde{w}_1 < -A_{22}) = Q\big(A_{22}\bar{\lambda}_1\big). \tag{68}$$

Hence,

$$\begin{aligned} \epsilon|\mathcal{C}_4 &= \frac{1}{2}\Pr(w_1[1] < -A_{10} \cup w_1[2] < -A_{10}) \\ &= Q(A_{10}\lambda_1) \end{aligned} \tag{69}$$

$$\begin{aligned} \varepsilon|\mathcal{C}_4 &= \frac{1}{2}\Pr(w_1[1] < -A_{12} \cup w_1[2] < -A_{12}) \\ &= Q(A_{12}\lambda_1). \end{aligned} \tag{70}$$

Consequently,

$$P_{B_1}^{\mathcal{C}_4} = Q(A_{10}\lambda_1) + Q\big(A_{22}\bar{\lambda}_1\big) \sum_{i \in \{0,2\}} (i-1) Q(A_{1i}\lambda_1). \tag{71}$$

By defining $\Psi(a) \triangleq Q(a\lambda_1)$ and $\Phi(a, b) \triangleq Q(a\lambda_1)Q(b\bar{\lambda}_1)$, the conditional BER for this configuration can be found by averaging the four cases such that

$$\begin{aligned} P_{B_1} &= \Psi(A_{10}) + \frac{1}{4}\left[\Psi\left(\frac{A_{\grave{2}2}}{\sqrt{\tau_1}}\right) + \Psi\left(\frac{A_{02}}{\sqrt{\tau_1}}\right)\right] \\ &\quad + 0.25[\Phi(A_{12}, A_{02}) + \Phi(A_{12}, A_{22})] \\ &\quad - 0.25\big[\Phi\big(A_{\grave{1}2}, A_{02}\big) + \Phi\big(A_{\grave{1}2}, A_{\grave{2}2}\big)\big] \\ &\quad - 0.25\big[\Phi\big(A_{10}, A_{\grave{2}2}\big) + 2\Phi(A_{10}, A_{02}) + \Phi(A_{10}, A_{22})\big]. \end{aligned} \tag{72}$$

Following a similar approach, the rest of the configurations can be found. The summary of the conditional BER expressions are summarized in Table 3. Interested readers can refer to the MATLAB code [35] to compute the BER expressions.

REFERENCES

[1] J. Li, H.-H. Chen, and Q. Guo, "On the performance of NOMA systems with different user grouping strategies," *IEEE Wireless Commun.*, vol. 31, no. 1, pp. 56–61, Feb. 2024.

[2] H. Yahya, A. Ahmed, E. Alsusa, A. Al-Dweik, and Z. Ding, "Error rate analysis of NOMA: Principles, survey and future directions," *IEEE Open J. Commun. Soc.*, vol. 4, pp. 1682–1727, 2023.

[3] H. Yahya, E. Alsusa, A. Al-Dweik, and M. Debbah, "Cognitive NOMA with blind transmission-mode identification," *IEEE Trans. Commun.*, vol. 71, no. 4, pp. 2042–2058, Apr. 2023.

[4] B. Clerckx et al., "Multiple access techniques for intelligent and multifunctional 6G: Tutorial, survey, and outlook," *Proc. IEEE*, early access, Jun. 18, 2024, doi: 10.1109/JPROC.2024.3409428.

[5] Z. Lin, M. Lin, J.-B. Wang, T. de Cola, and J. Wang, "Joint beamforming and power allocation for satellite-terrestrial integrated networks With non-orthogonal multiple access," *IEEE J. Sel. Topics Signal Process.*, vol. 13, no. 3, pp. 657–670, Jun. 2019.

[6] Z. Lin, M. Lin, T. de Cola, J.-B. Wang, W.-P. Zhu, and J. Cheng, "Supporting IoT with rate-splitting multiple access in satellite and aerial-integrated networks," *IEEE Internet Things J.*, vol. 8, no. 14, pp. 11123–11134, Jul. 2021.

[7] Z. Lin, M. Lin, B. Champagne, W.-P. Zhu, and N. Al-Dhahir, "Secrecy-energy efficient hybrid beamforming for satellite-terrestrial integrated Networks," *IEEE Trans. Commun.*, vol. 69, no. 9, pp. 6345–6360, Sep. 2021.

[8] K. An et al., "Exploiting multi-layer refracting RIS-assisted receiver for HAP-SWIPT networks," *IEEE Trans. Wireless Commun.*, early access, May 3, 2024, doi: 10.1109/TWC.2024.3394214.

[9] S. McWade, M. F. Flanagan, L. Zhang, and A. Farhang, "Interference and rate analysis of multinumerology NOMA," in *Proc. IEEE ICC*, Dublin, Ireland, 2020, pp. 1–6.

[10] S. McWade, M. F. Flanagan, J. Mao, L. Zhang, and A. Farhang, "Resource allocation for mixed numerology NOMA," *IEEE Wireless Commun. Lett.*, vol. 10, no. 10, pp. 2240–2244, Oct. 2021.

[11] J. Choi, B. Kim, K. Lee, and D. Hong, "A transceiver design for spectrum sharing in mixed numerology environments," *IEEE Trans. Wireless Commun.*, vol. 18, no. 5, pp. 2707–2721, May 2019.

[12] N. Shi et al., "Peak-to-average power ratio reduction using selected mapping for mixed numerology NOMA," *IEEE Trans. Wireless Commun.*, early access, Mar. 28, 2024, doi: 10.1109/TWC.2024.3380349.

[13] T. V. S. Sreedhar and N. B. Mehta, "Inter-numerology interference in mixed numerology OFDM systems in time-varying fading channels with phase noise," *IEEE Trans. Wireless Commun.*, vol. 22, no. 8, pp. 5473–5485, Aug. 2023.

[14] B. Kim, Y. Park, and D. Hong, "Partial non-orthogonal multiple access (P-NOMA)," *IEEE Wireless Commun. Lett.*, vol. 8, no. 5, pp. 1377–1380, Oct. 2019.

[15] B. Kim, J. Heo, and D. Hong, "Partial non-orthogonal multiple access (P-NOMA) with respect to user fairness," in *Proc. IEEE VTC*, Honolulu, HI, USA, 2019, pp. 1–5.

[16] K. S. Ali, E. Hossain, and M. J. Hossain, "Partial non-orthogonal multiple access (NOMA) in downlink Poisson networks," *IEEE Trans. Wireless Commun.*, vol. 19, no. 11, pp. 7637–7652, Nov. 2020.

[17] K. S. Ali et al., "Meta distribution of partial-NOMA," *IEEE Wireless Commun. Lett.*, vol. 11, no. 12, pp. 2695–2699, Dec. 2022.

[18] B. Zhuo et al., "Partial non-orthogonal multiple access: A new perspective for RIS-aided downlink," *IEEE Wireless Commun. Lett.*, vol. 11, no. 11, pp. 2395–2399, Nov. 2022.

[19] B. Zhuo et al., "Partial-NOMA based physical layer security: Forwarding design and secrecy analysis," *IEEE Trans. Intell. Transp. Syst.*, vol. 24, no. 7, pp. 7471–7484, Jul. 2023.

[20] K. S. Ali, A. Al-Dweik, E. Hossain, and M. Chafii, "Physical layer security of partial-NOMA and NOMA in Poisson networks," *IEEE Trans. Wireless Commun.*, vol. 23, no. 6, pp. 6562–6579, Jun. 2024.

[21] B. Zhuo et al., "Partial-NOMA based PLS: Following NOMA decoding principle or enhanced decoding design?" *IEEE Trans. Veh. Technol.*, vol. 72, no. 10, pp. 13637–13642, Oct. 2023.

[22] M. W. Akhtar, A. Mahmood, and M. Gidlund, "Partial NOMA for semi-integrated sensing and communication," in *Proc. IEEE GC Workshops*, Kuala Lumpur, Malaysia, 2023, pp. 1129–1134.

[23] Y. Chi et al., "Variable-rate coding with constant BER for NOMA via multilevel IRA coding," *IEEE Trans. Veh. Technol.*, vol. 68, no. 5, pp. 5149–5153, May 2019.

[24] A. Al-Dweik, E. Alsusa, O. A. Dobre, and R. Hamila, "Multi-symbol rate NOMA for improving connectivity in 6G communications networks," *IEEE Commun. Mag.*, vol. 62, no. 7, pp. 118–123, Jul. 2024.

[25] J. Mao, L. Zhang, P. Xiao, and K. Nikitopoulos, "Interference analysis and power allocation in the presence of mixed numerologies," *IEEE Trans. Wireless Commun.*, vol. 19, no. 8, pp. 5188–5203, Aug. 2020.

[26] M. Yang, J. Chen, Z. Ding, Y. Liu, L. Lv, and L. Yang, "Joint power allocation and decoding order selection for NOMA systems: Outage-optimal strategies," *IEEE Trans. Wireless Commun.*, vol. 23, no. 1, pp. 290–304, Jan. 2024.

[27] H. Yahya, E. Alsusa, and A. Al-Dweik, "Exact BER analysis of NOMA with arbitrary number of users and modulation orders," *IEEE Trans. Commun.*, vol. 69, no. 9, pp. 6330–6344, Sep. 2021.

[28] Y. Iraqi and A. Al-Dweik, "Power allocation for reliable SIC detection of rectangular QAM-based NOMA systems," *IEEE Trans. Veh. Technol.*, vol. 70, no. 8, pp. 8355–8360, Aug. 2021.

[29] H. Lee, I. Jung, J. Heo, and D. Hong, "Exploiting intentional time-domain offset in downlink multicarrier NOMA systems," *IEEE Wireless Commun. Lett.*, vol. 10, no. 7, pp. 1577–1580, Jul. 2021.

[30] J. Son, H. Lee, I. Jung, and D. Hong, "Exploiting intentional frequency offset in NOMA-OFDM systems: From basic to practical," *IEEE Trans. Wireless Commun.*, vol. 22, no. 10, pp. 7087–7097, Oct. 2023.

[31] X. Zhang, L. Zhang, P. Xiao, D. Ma, J. Wei, and Y. Xin, "Mixed numerologies interference analysis and inter-numerology interference cancellation for windowed OFDM systems," *IEEE Trans. Veh. Technol.*, vol. 67, no. 8, pp. 7047–7061, Aug. 2018.

[32] M. Ganji and H. Jafarkhani, "Time asynchronous NOMA for downlink transmission," in *Proc. IEEE WCNC*, Marrakesh, Morocco, 2019, pp. 1–6.

[33] H. Yahya, E. Alsusa, and A. Al-Dweik, "Design and analysis of NOMA with adaptive modulation and power under BLER constraints," *IEEE Trans. Veh. Technol.*, vol. 71, no. 10, pp. 11228–11233, Oct. 2022.

[34] P. J. Dhrymes, "Matrix vectorization," in *Mathematics for Econometrics*. New York, NY, USA: Springer, 2000, pp. 117–145.

[35] H. Yahya, E. Alsusa, and A. Al-Dweik. "BER performance of multirate-NOMA." Feb. 2024. [Online]. Available. https://codeocean.com/capsule/7273838/tree/v1

HAMAD YAHYA (Member, IEEE) was born in Sharjah, UAE, in 1997. He received the M.Sc. degree (with Distinction) in communications and signal processing and the Ph.D. degree in electrical and electronic engineering from The University of Manchester, Manchester, U.K., in 2019 and 2023, respectively.

He is currently enrolled in the UAE National Postdoctoral Fellowship Program with Khalifa University. He is also a Visiting Researcher with the Communications and Signal Processing Research Group, Imperial College London, U.K. Prior joining Khalifa University, he worked as a Research Associate with the Communication Systems Research Group, The University of Manchester, where he was the Co-Founder and the Chair of the IEEE ComSoc SBC. His research interests include wireless communications for future wireless networks, optimization, and visible light communication. He received the Best Student and the Best Project Prizes from the Department of Electrical and Electronic Engineering, The University of Manchester. He was nominated for the Distinguished Achievement Award in 2019, where he was among the top 14 postgraduate taught students across the Faculty of Science and Engineering. He is the recipient of the M.Sc. Success Scholarship from The University of Manchester.

EMAD ALSUSA (Senior Member, IEEE) received the Ph.D. degree in telecommunications from the University of Bath, U.K., in 2000. In 2000, he joined with Edinburgh University, working on high data rate systems within an industrial project. He joined Manchester University in September 2003, where is currently a Professor of Wireless Communications and Signal Processing and the Head of the Communications Research Group. He has authored over 300 journals and refereed conference publications, prominently featured in top IEEE transactions and conferences. He has successfully supervised over 40 Ph.D. students. His research focuses on communication systems, specifically in the physical, MAC, and network layers for which he develops techniques and algorithms, such as array signal detection, channel estimation, equalization, adaptive signal precoding, interference avoidance, radio resource management, and energy and spectrum optimization. His research finds applications in cellular networks, IoT, Industry 4.0, vehicular networks, and powerline communications. He has received several awards, including the Best Paper Award at the International Symposium on Power Line Communications in 2016 and the Wireless Communications and Networks Conference in 2019. He serves as an Editor for IEEE WIRELESS COMMUNICATIONS LETTERS and the IEEE TRANSACTIONS ON VEHICULAR TECHNOLOGY. He has held roles as the TPC Track Chair for conferences, such as VTC'16, GISN'16, PIMRC'17, and Globecom'18, and served as the General Co-Chair for the OnlineGreenCom'16 Conference. He is currently the U.K. in the International Union of Radio Science and the Co-Chair the IEEE Special Working Group on RF Energy Harvesting. He is a Fellow of the U.K. Higher Academy of Education.

ARAFAT AL-DWEIK (Senior Member, IEEE) received the M.S. (summa cum laude) and Ph.D. (magna cum laude) degrees in electrical engineering from Cleveland State University, Cleveland, OH, USA, in 1998 and 2001, respectively. He was with Efficient Channel Coding Inc., Cleveland, the Department of Information Technology, Arab American University, Jenin, Palestine, and the University of Guelph, Guelph, ON, Canada. He is currently with the Department of Computer and Information Engineering, Khalifa University, Abu Dhabi, UAE. He is also a Visiting Research Fellow with the School of Electrical, Electronic, and Computer Engineering, Newcastle University, Newcastle upon Tyne, U.K., and a Research Professor with Western University, London, ON, Canada, and the University of Guelph. He has extensive research experience in various areas of wireless communications that include modulation techniques, channel modeling and characterization, synchronization and channel estimation techniques, OFDM technology, error detection and correction techniques, MIMO, and resource allocation for wireless networks. He was the recipient of the UAE Lead-er-Founder Award in 2019, the Dubai Award for Sustainable Transportation in 2016, the Hijjawi Award for Applied Sciences in 2003, and the Fulbright Alumni Development Grant in 2003 and 2005. He was awarded the Fulbright Graduate Student Scholarship from 1997 to 1999. Since 2012, he has been an Editor of IEEE TRANSACTIONS ON VEHICULAR TECHNOLOGY. He was an Associate Editor of the *IET Communications* from 2015 to 2020. He has been an Associate Editor of *Frontiers in Communications and Networks* since 2021. He is a registered Professional Engineer in the Province of Ontario, Canada. He is a Distinguished Lecturer of the IEEE from 2023 to 2025. He is a member of Tau Beta Pi and Eta Kappa Nu.